Earth-Science Reviews 250 (2024) 104717

Contents lists available at ScienceDirect

Earth-Science Reviews

journal homepage: www.elsevier.com/locate/earscirev

Carbon dynamics shift in changing cryosphere and hydrosphere of the Third Pole

Tanguang Gao [a], Shichang Kang [b,g], Tandong Yao [c], Yanlong Zhao [a], Xuexue Shang [a], Yong Nie [d], Rensheng Chen [e], Igor Semiletov [f,h], Taigang Zhang [a], Xi Luo [b,g], Da Wei [d,*], Yulan Zhang [b,*]

[a] College of Earth and Environmental Sciences, Lanzhou University, Lanzhou 730000, China
[b] State Key Laboratory of Cryospheric Science, Northwest Institute of Eco-Environment and Resources, Chinese Academy of Sciences, Lanzhou 730000, China
[c] State Key Laboratory of Tibetan Plateau Earth System, Environment and Resources, Institute of Tibetan Plateau Research, Chinese Academy of Sciences, Beijing 100101, China
[d] Key Laboratory of Mountain Surface Processes and Ecological Regulation, Institute of Mountain Hazards and Environment, Chinese Academy of Sciences, Chengdu 610041, China
[e] Qilian Alpine Ecology and Hydrology Research Station, Key Laboratory of Inland River Ecohydrology, Northwest Institute of Eco−Environment and Resources, Chinese Academy of Sciences, Lanzhou 730000, China
[f] Pacific Ocedanological Institute, Far Eastern Branch of the Russian Academy of Sciences, Vladivostok 690043, Russia
[g] University of Chinese Academy of Sciences, Beijing 100049, China
[h] National Tomsk Research State University, Tomsk 634050, Russia

ARTICLE INFO

Keywords:
Cryosphere
Permafrost thawing
Glacier melting
Carbon release
Third Pole

ABSTRACT

The Third Pole (TP) is the largest alpine mountains on the Earth. Its cryosphere is shrinking and collapsing and the hydrosphere has subsequently changed under the warming climate in recent decades, potentially affecting the biogeochemical cycle. In particular, the carbon cycle has undergone dramatic changes, primarily because of the alterations between the cryosphere and hydrosphere. Carbon emissions from melting glaciers and thawing permafrost can trigger climate change feedback. However, carbon dynamics linked to the changes of cryosphere and hydrosphere under climate warming on the TP still require clarification comprehensively. Herein, we reviewed the current state of carbon stocks in the changing TP cryosphere and hydrosphere, focusing on their variations in permafrost, glaciers, and related inland waters (headwater rivers, thermokarst lakes, and glacial lakes). We also revealed the carbon release pathways into aquatic ecosystems and the atmosphere. Finally, we recommended research priorities to address the dynamics of carbon cycling and its possible future impacts on the TP. This review highlights the importance of carbon cycle dynamics in the TP under future climate change.

1. Introduction

As an essential cryospheric region at mid-low latitudes, the Third Pole (TP), including the core region of the Tibetan Plateau, Tien Shan, Hindu Kush, Karakoram, and the Himalayan Mountain range, has the largest storage of frozen water after the polar regions (Fig. 1) (Yao et al., 2012). With great areas of glaciers, permafrost, and high-altitude lakes, the TP cryosphere and hydrosphere are called the “Asian Water Tower” (Immerzeel et al., 2020; Immerzeel et al., 2010; Yao et al., 2022). Several prominent Asian Rivers (e.g., the Yellow, Yangtze, Brahmaputra, Ganges, and Indus) originate from meltwater on the TP and supply water to approximately one billion people in the downstream regions (Azam et al., 2021; Immerzeel et al., 2010; Li et al., 2022a; Nie et al., 2021). Recently, the TP cryosphere has experienced rapid shrinkage, resulting in enhanced glacial melting, abrupt permafrost thawing, increased river runoff, and extended lake areas (Brun et al., 2018; Farinotti et al., 2019; Gao et al., 2021b; Yao et al., 2022; Zhang et al., 2022). Such changes influence the regional hydrological cycle and water resources, causing the TP hydrosphere imbalance (Gao et al., 2021a; Huss and Hock, 2018; Immerzeel et al., 2010; Yao et al., 2022). More importantly, these changes profoundly affect carbon cycling across the entire TP recently (Chen et al., 2022; Wei et al., 2021b).

TP glaciers and permafrost contain a large amount of carbon (Ding et al., 2019; Mu et al., 2020). Previous studies have estimated the dissolved organic carbon (DOC) stored in glaciers (Li et al., 2018b; Liu et al., 2016). The permafrost soil organic carbon (SOC) stock over the TP

* Corresponding authors.
E-mail addresses: weida@imde.ac.cn (D. Wei), yulan.zhang@lzb.ac.cn (Y. Zhang).

https://doi.org/10.1016/j.earscirev.2024.104717
Received 1 November 2023; Received in revised form 3 February 2024; Accepted 16 February 2024
Available online 17 February 2024

fluctuates significantly with high uncertainties and is impacted by the in situ observed SOC data, temperature, precipitation, vegetation, and the topographic landscape (Mishra et al., 2021b). Owing to rapid climate warming and cryospheric melting, carbon stored in glaciers and permafrost can be re-released into aquatic ecosystems and the atmosphere. However, determining the pathways and constraining the amount of carbon released into the hydrosphere and atmosphere remain large uncertainty. Modeling studies have attempted to project the quantity of DOC or SOC that will be released when glaciers melt or permafrost thaws (Hood et al., 2015; Natali et al., 2021). In particular, the dramatic abrupt thawing of permafrost (thermokarst landscapes) owing to climate warming can accelerate SOC release (Gao et al., 2021b; Liu et al., 2018; Turetsky et al., 2019; Yang et al., 2018). The degradation of permafrost has complex consequences for greenhouse gases (GHGs) dynamics in the TP as well as in the Arctic climate system (Yang et al., 2018). The biogeochemical and physical processes of permafrost on the TP has been operated at various temporal and spatial scales, which can trigger large scale feedback and have interactions with the Earth system. It is critical to understand these processes and their interactions between the physical, biogeochemical, and human dimensions on the TP (Chen et al., 2022). It is also a challenge to analyze and identify similarities and differences in the responses of TP permafrost and climate systems to variability of temperature and moisture (Wang et al., 2023). Some feedback mechanisms, such as energy and water exchange operate at local to regional scales whereas others, particularly the mobilization and transformation of carbon, and the GHG fluxes from different types of thawing permafrost, have the potential to operate at regional and global scales (Liu et al., 2018; Yang et al., 2023; Yang et al., 2018).

In addition to lateral carbon transport from glaciers and permafrost to the hydrosphere, a significant amount of carbon-related GHGs (i.e., CO_2 and CH_4) are emitted into the atmosphere from permafrost thawing and glacial basins (Karlsson et al., 2021; Serikova et al., 2019; Wadham et al., 2012). GHGs has been observed to be released from the deep permafrost in the northern Tibetan Plateau (Mu et al., 2018). The thermokarst lakes and permafrost collapse on the TP outgas large amounts of CH_4 into the atmosphere (Mu et al., 2023; Mu et al., 2016; Wang et al., 2021b; Yang et al., 2018). A study on the Greenland ice sheet indicated that the ice sheet bed can continuously export CH_4-supersaturated water during the melt season (Lamarche-Gagnon et al., 2019). Along the boundaries of the Arctic, permafrost thawing and glaciers melting can facilitate the transient expulsion of CH_4 trapped by the cryosphere (Anthony et al., 2012), playing a potential effect on formation of the Arctic planetary atmospheric maximum for CH_4 and CO_2 (Semiletov, 1999). Glacial cryoconite holes on the TP may also play an important role in CH_4 emissions (Zhang et al., 2021b). These emissions substantially influence the net ecosystem carbon balance over the TP (Chen et al., 2022; Wei et al., 2021b).

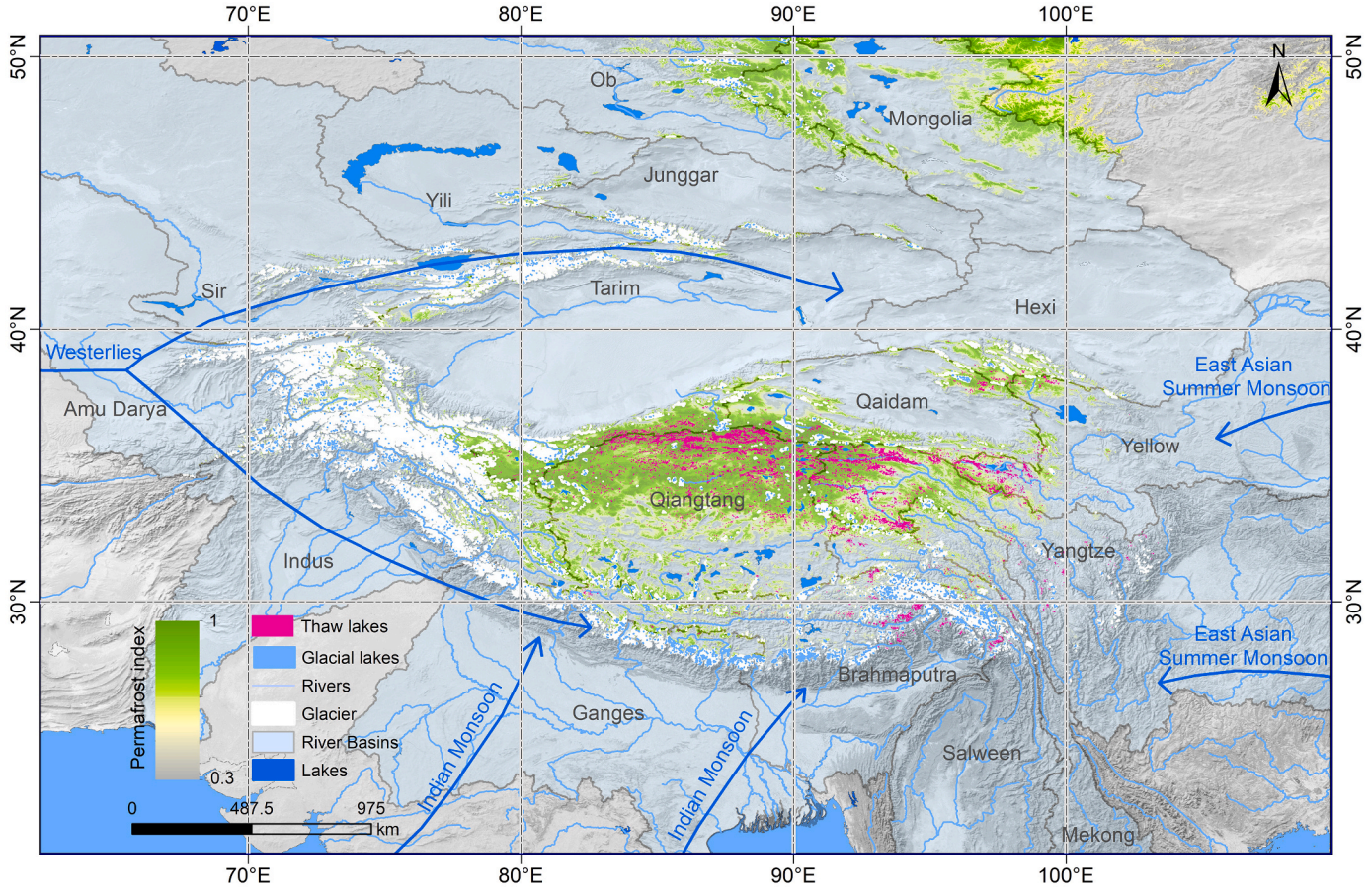

Fig. 1. Distributions of glaciers, glacial lakes, permafrost, thermokarst lakes, and lakes and river basins across the Third Pole. The TP includes >90,000 glaciers, with a total area of approximately 97,590 km^2 (Farinotti et al., 2019). Intense glacier retreat and melting have formed numerous glacial lakes on the TP, indicating the potential for 15,826 glacial lakes covering 2253.95 km^2 with a water volume of 60.49 km^3 (Zhang et al., 2022). The permafrost covers approximately 1.06–1.48 million km^2 (Zhao et al., 2018; Zou et al., 2017). Thermokarst lakes form and develop on the TP due to rapid permafrost thaw, yielding a total of approximately 161,300 thaw lakes with sizes ranging from 500 m^2 to 3 km^2 and a total area of approximately 2825.45 ± 5.75 km^2 (Wei et al., 2021c). The area of lakes (larger than 1 km^2) in 2018 was approximately 50,000 km^2 (Zhang et al., 2019). Melting water from glaciers and permafrost is the source of several prominent rivers in Asia (e.g., Yellow, Yangtze, Brahmaputra, Ganges, and Indus) with a total runoff of 565 Gt yr^{-1} (Wang et al., 2021c), which also results in the extension of lakes (Yao et al., 2022). (For interpretation of the references to colour in this figure legend, the reader is referred to the web version of this article.)

Rivers and lakes are essential inland water bodies that release GHGs (Raymond et al., 2013; Rosentreter et al., 2021). Freshwater, brackish lakes, and headwater rivers on the TP are affected by glacial meltwater and permafrost thawing (Immerzeel et al., 2010; Nie et al., 2021; Wang et al., 2021c; Zhang et al., 2019). OC release from Tibetan permafrost thawing can be transported into aquatic systems, consequently affecting GHGs emissions (Qu et al., 2017a; Qu et al., 2017b). Generally, the fate of carbon entering rivers includes outgassing, burial, and downstream transport (to the ocean) (Ran et al., 2015). Headwater rivers are also a significant source of GHGs (Li et al., 2021a; Zhang et al., 2020). Lakes on the TP, which are substantially influenced by cryospheric melting, are atmospheric conduits of GHGs (Xun et al., 2022; Yan et al., 2018).

The TP cryosphere constitutes a critical linkage between the terrestrial, aquatic, and atmospheric carbon fluxes. In the TP cryosphere, glaciers and permafrost can be characterized by the long-term accumulation of carbon through dry and wet deposition (Ding et al., 2019). Under rapid climate warming and cryosphere retreat, lateral and vertical transport and carbon emissions have increased in recent decades. Thermokarst lakes and headwater rivers in the TP are hotspots for carbon transport downstream and into the atmosphere (Mu et al., 2023; Zhang et al., 2020). This indicates that cryospheric and hydrospheric changes have profoundly impacted the regional carbon cycles (Chen et al., 2022). However, studies have yet to comprehensively combine carbon stocks and release from glaciers, permafrost, lakes, and headwater rivers across the TP. Their contributions to the net ecosystem carbon balance over the TP must be further analyzed based on detailed data. Therefore, to improve our understanding of the impacts of cryospheric melting on regional carbon cycles, it is critical to forecast responses to current and future climate changes.

In this review, we have synthesized current cryosphere related carbon data over the TP and highlight the significance of carbon stocks and releases associated with changes in the cryosphere and hydrosphere across the TP. Specifically, based on the literature and datasets of DOC, particulate organic carbon (POC), black carbon (BC), and GHGs from glaciers, as well as data on SOC, POC, and GHGs from permafrost regions, and GHG emissions data from headwater rivers and lakes, we review the state of knowledge on carbon stocks in glaciers, permafrost, and thermokarst lakes. We discuss the release of carbon into rivers and the atmosphere on the TP. We also evaluate how cryosphere and hydrosphere changes likely affect carbon cycling over the TP. Furthermore, based on current knowledge, we recommend future research directions for integrated cryospheric and hydrospheric changes and carbon dynamics. To fill these critical gaps, a collective effort is required to quantify the climate effects of carbon released from permafrost and glacier melting in the future.

2. Permafrost carbon storage and release

Permafrost is the ground with a temperature at or below 0 °C for at least two consecutive years. The Earth's permafrost carbon is mainly distributed in the Arctic and TP regions, depending on regional and global climate conditions, ecosystem dynamics, and anthropogenic activities in permafrost regions (Mishra et al., 2021b; Nitze et al., 2018). The permafrost contains a massive frozen storage of organic carbon (approximately 1600 Pg of carbon and 1079 Pg C in the top 3 m of the soil), which is equal to the amount of carbon in the Earth's atmosphere (Hugelius et al., 2014; McGuire et al., 2016; Mishra et al., 2021b; Schuur et al., 2015; Wu et al., 2022; Zimov et al., 2006). The warming and thawing of permafrost promote the decomposition of frozen organic carbon, threatening regional climate change and carbon cycles (Natali et al., 2021; Olefeldt et al., 2016; Turetsky et al., 2020). Previous studies have indicated that the lateral transport of thawed permafrost carbon from land to rivers and oceans translocates GHGs released from thawing sites (Abbott and Jones, 2015; Vonk et al., 2015). Meanwhile, permafrost thawing is one of only a few processes that can move significant quantities of SOC into the aquatic ecosystem and atmosphere in response to a changing climate on short timescales (Miner et al., 2021; Schuur et al., 2015; Turetsky et al., 2020). Substantial permafrost carbon releases and emissions provide a rapid and significant positive feedback loop for climate change (Miner et al., 2022; Natali et al., 2021; Vonk et al., 2015), which has been further highlighted by the Sixth Assessment Report of Intergovernmental Panel on Climate Change (IPCC AR6) (IPCC, 2021).

2.1. Carbon storage in TP permafrost

Recent studies have examined the distribution and amount of permafrost SOC in the TP. Accurate estimations of the storage and distribution of permafrost SOC are vital for investigating the regional carbon cycle and its potential impacts on climate and the environment (Mu et al., 2020; Wang et al., 2023). Previous studies have conducted large-scale field-scaling observations of soil pits and cores (Fig. S1) (Wang et al., 2021a). The spatial distribution of SOC stocks at different depth intervals reveals an overall decreasing trend from the southeast to the northwest of the TP (Fig. 2a and b) (Ding et al., 2019; Wang et al., 2021a). Wetland regions in the eastern TP hold the greatest SOC stocks for soil depths of 0–3 m (> 32 kg m^{-2}), whereas the northern TP (the Qiangtang and Qaidam basins) had the lowest SOC stock (< 8 kg m^{-2}). Generally, SOC stocks decrease with increasing soil depth (Gao et al., 2021b; Wang et al., 2021a). Approximately half of the SOC has been predicted to occur in surface soils with depths of 0–1 m (Mishra et al., 2021b). The uppermost 30 cm soil accounts for 34.26% of SOC storage at depths of 0–3 m, with only approximately 17% stored at depths of 2–3 m (Mishra et al., 2021b; Wang et al., 2021a). Diverse environmental factors, including surface air and soil temperatures, soil wetness, precipitation, topographic attributes, elevation, and slope angle, profoundly influence the heterogeneity of SOC stocks in different permafrost regions and depth intervals (Mishra et al., 2021b).

Permafrost on the TP covers an area of approximately 1.06×10^6–1.086×10^6 km^2 (Zou et al., 2017). TP permafrost contains approximately 14.4–40.9 Pg SOC in the top 3 m of soil based on different methods (Table S1 and Fig. 2c). For example, the modern soil carbon storage in permafrost is estimated to be approximately 36.6 Pg C at depths of 0–3 m based on machine learning techniques that account for paleoclimatic effects; this data is triple that predicted result by the 11 ecosystem models (11.5 Pg C) (Ding et al., 2019). A machine learning approach provided an estimate of carbon storage of approximately 21.69–24.49 Pg C at depth of 0–3 m (Wang et al., 2021a). Upscaled by soil classification, the permafrost SOC is estimated to be approximately 40.9 Pg C (Jiang et al., 2019). The SOC calculated using the Random Forest and regression−kriging methods is 21.8 and 14.4 Pg C, respectively (Mishra et al., 2021b; Wu et al., 2022). The contributions of POC, mineral-associated organic carbon (MAOC), and iron-bound organic carbon (Fe-OC) are approximately 6.34%, 40.81%, and 6.78%, respectively (Liu et al., 2022a). Therefore, estimated storage is approximately 0.91–2.59 Pg C − POC, 5.88–16.69 Pg C − MAOC, and 0.98–2.77 Pg C − Fe − OC.

The alpine permafrost of the TP is formed under very different climatic conditions compared with the Arctic permafrost. The Arctic permafrost is formed by weak solar radiation, particularly in winter. In contrast, alpine permafrost is formed at high altitudes and with much lower latitudes, that is 25–45°N, where there is strong solar radiation. Consequently, this unique climate determines alpine permafrost carbon. For example, strong solar radiation on the TP induces higher gross primary productivity (~700 g C m^{-2} yr^{-1}) (Wei et al., 2021a), compared with that in the Arctic (~400 g C m^{-2} yr^{-1}) (Li et al., 2021c). The active layer thickness is 203 cm on the TP and ~ 100 cm on Arctic permafrost (Wang et al., 2022b). Strong solar radiation also causes a rapid turnover time and shallow soil depth of the alpine permafrost on the TP (You et al., 2021), largely determining its carbon content, that is the soil carbon density of the TP accounts only 20% of its Arctic counterparts for the 0–3 m soil column (Mishra et al., 2021a). The most carbon-rich soil

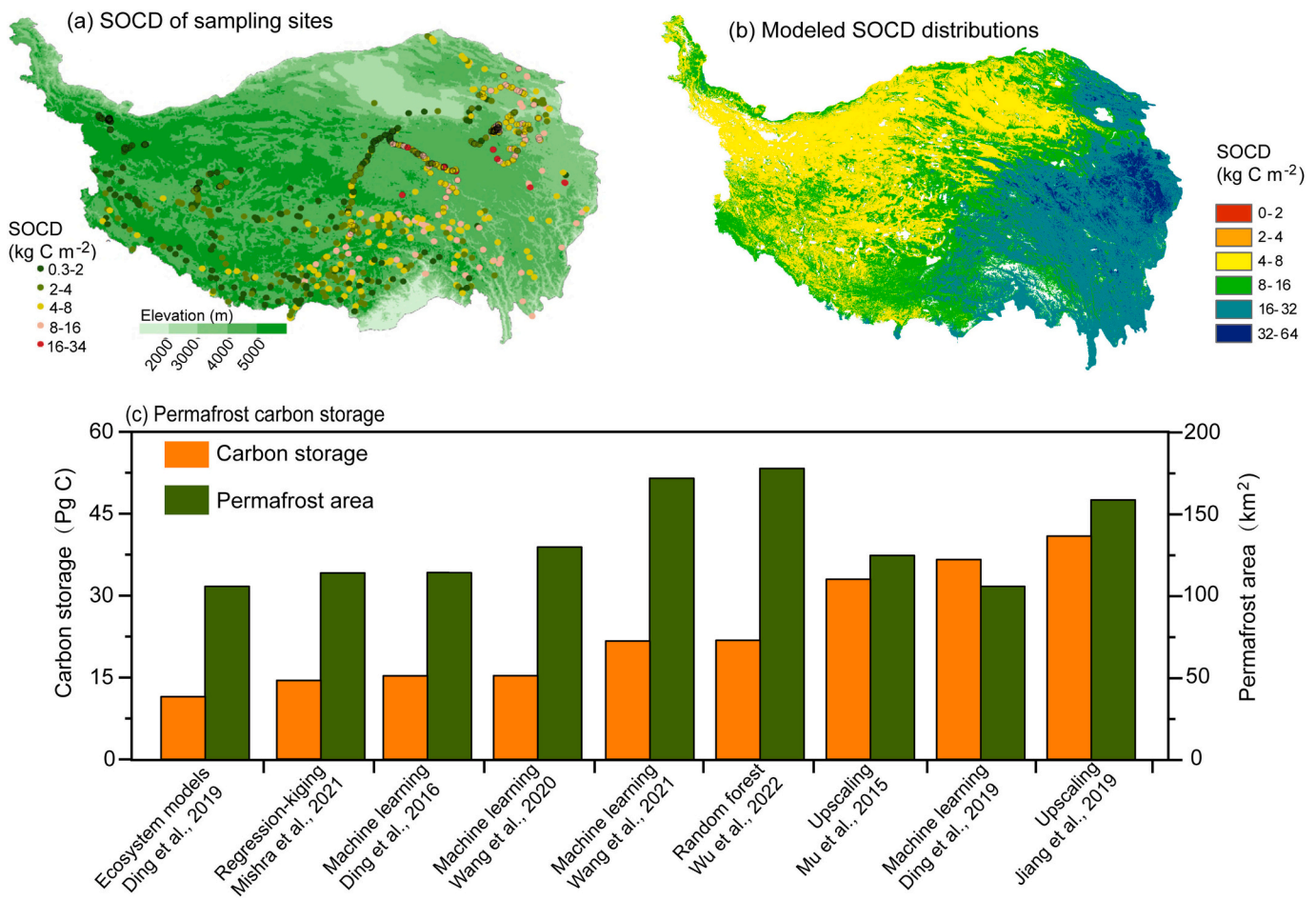

Fig. 2. Distribution of soil organic carbon across the core region of the Third Pole. (a) Locations and soil organic carbon density (SOCD) of the top 30 cm layer for the 1114 sampling sites (Ding et al., 2019), (b) modeled spatial distribution of soil organic carbon stocks (SOCS) at a depth of 0–3 m (Wang et al., 2021a), and (c) carbon storage by different analysis methods and s permafrost areas on the Third Pole (Table S1).

layer (0–1 m) of the TP (6–9.5 kg C m^{-2}) is even less dense than the 2–3 m soil layer of the Arctic permafrost (6–10 kg C m^{-2}). The 0–2 m soil layer accounts for 87% of SOC storage at depths of 0–3 m on the TP (Wang et al., 2021a), indicating that most SOC is within the range of active soil layers (203 cm on the TP), whereas <13% SOC is buried in the deep-frozen soil layers. In the Arctic, over 50% of SOC is buried in permafrost soil layers (~1 m). The difference in the soil profile with respect to SOC inevitably affects its feedback on climate warming.

Thermokarst dynamics combined with SOC characteristics control the release of carbon from permafrost soil (Weiss et al., 2016). Sedimentary SOC storage in thermokarst lakes and ponds across the TP permafrost region is significant because of the rapid increase in their number and area (Wei et al., 2021c). However, they are highly vulnerable to climate change. The estimated top 3 m of sedimentary soil in thermokarst lakes across the TP, with data from 152 1-m-deep cores and 32 0.5-m-deep cores, indicates that the sedimentary SOC stock is approximately 52.62 Tg in the top 3 m, with 53% of the SOC stored in the upper 1 m (Wei et al., 2022). The sedimentary carbon density of these thermokarst lakes is higher than that of the surrounding permafrost soil at different depths (Wei et al., 2022).

2.2. SOC loss due to permafrost thawing

With climate warming, substantial carbon loss due to permafrost thawing has been observed during the past decade (Schuur et al., 2009; Turetsky et al., 2020). Under RCP4.5 and RCP8.5, Northern Hemisphere permafrost thawing will induce carbon emissions ranging from 6 to 33 Pg and 23 to 174 Pg C by 2100, respectively (Anthony et al., 2018; MacDougall et al., 2012; Schuur et al., 2015). Such emissions will potentially offset the global land carbon sink by approximately 160 Pg by 2100 (Friedlingstein et al., 2006).

Rapid permafrost degradation occurs on the TP under climate warming, with the deepening active layer, increases soil temperature, and more frequent thermokarst occurrences (Gao et al., 2021b; Shen et al., 2023; Wang et al., 2021a; Wei et al., 2022; Yang et al., 2019; Zhao et al., 2020). In particular, the active layer depth over the TP permafrost region is projected to increase by 0.71 and 1.53 m by the 2090s under RCP4.5 and RCP8.5, respectively (Wang et al., 2020). Meanwhile, significant decreases in permafrost areas (22% to 64%) are projected under future climate warming scenarios in the TP permafrost region (Lu et al., 2017). With continuous warming, permafrost thawing is projected to result in ~1.86 ± 0.49 Pg and ~ 3.80 ± 0.76 Pg of carbon loss by 2100 under RCP4.5 and RCP8.5, respectively (Wang et al., 2020).

The dramatic abrupt thawing of permafrost (e.g., permafrost collapse, gully erosion, or thermokarst lakes) due to climate warming is accelerating carbon release. In the eastern TP, permafrost collapses have lost approximately 23%–37% of their SOC concentrations per decade since the early 2000s, corresponding to an approximately 15%–20% reduction in the carbon stock of the top 30 cm of soil (Fig. 3a and b) (Gao et al., 2021b). Permafrost collapses in the northeastern TP have resulted in a 21% decrease in the SOC concentration and a 32% reduction in the carbon stock in the top 15 cm of soil over past 16 years (Fig. 3c and d) (Liu et al., 2018). A recent study on the permafrost thaw sequence and thermokarst impacted sites on the TP topsoil reveals that the thermos-

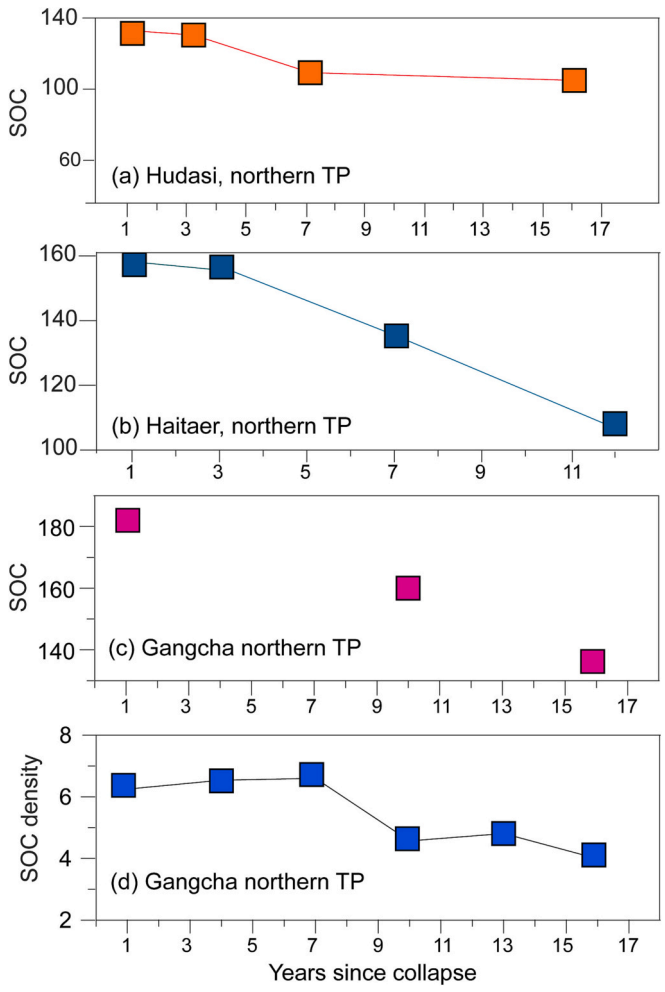

Fig. 3. Changes in the soil carbon by year since permafrost collapse on the Third Pole. SOC (g kg^{-1}) data in (a) and (b) from (Gao et al., 2021b); SOC and SOC density (kg m^{-2}) data in (c) and (d) from (Liu et al., 2018).

erosion gully-induced particulate organic carbon content has substantially decreased. In contrast, the mineral-related organic carbon content remain stable and iron−bound organic carbon (OC-Fe) accumulates because of the enrichment of Fe oxides after permafrost thawing (Liu et al., 2022a). The degradations have significantly affected the hydrological processes (Gao et al., 2018; Li et al., 2020b), carbon cycles (Chen et al., 2022; Gao et al., 2021b; Mu et al., 2020), and thermodynamic processes (Zhao et al., 2021). These consequences will provide vital feedback on future regional climate change (Wang et al., 2021c; Zhang et al., 2020).

2.3. GHG emissions

Most permafrost-thawed carbon can be converted to GHGs, such as CO_2 and CH_4, which can be a substantial carbon source to the atmosphere (Turetsky et al., 2020). In the northern TP, GHG production in deep permafrost is mainly related to the C:N ratios and stable isotopes of SOC (Mu et al., 2018). Other studies have indicated that CO_2-C release from both the active layer and permafrost deposits is significantly associated with environmental variables (soil moisture, soil pH, and temperature), microbial abundance (bacterial phospholipid fatty acids (PLFAs), fungal PLFAs, and actinomycin PLFAs), and carbon quality (described by a matrix of C:N, lignin-, cutin-, and suberin-derived compounds, as well as different carbon fraction pool sizes) (Chen et al., 2016; Qin et al., 2021). During an 80 d laboratory incubation period, the CO_2-C release rate from the active layer and permafrost deposits on the TP ranged from 116 to 223 μg CO_2-C g^{-1} OC d^{-1} (Chen et al., 2016). By 2100, either 111–146 Tg C (RCP4.5) or 281–369 Tg C (RCP8.5) could be released into the atmosphere as CO_2 from TP permafrost (Schuur et al., 2013). At permafrost thaw sequence on the TP during peak growing season, CH_4 emission ranges from 0.2 to 1.33 mg CH_4 m^{-2} h^{-1}, with a relatively high emission rate in the late thaw stage (Yang et al., 2018). The number and area of permafrost retrogressive thaw slumps (including permafrost thaw sequences and collapses) in the permafrost regions of the TP have significantly increased over the last 12 years (2008–2020) (Gao et al., 2021b; Luo et al., 2022). Active permafrost retrogressive thaw slumps are mainly concentrated in the central TP, with 2669 items and a total area of 38.4336 km^2 based on Gaofen satellite images (Luo et al., 2022). Estimated CH_4 emissions from permafrost retrogressive thaw slumps are approximately 0.037–0.245 Gg C yr^{-1} (Table S2). Together, these results suggest that carbon release from the TP permafrost to the atmosphere could outweigh the potential carbon gain by plants in the TP permafrost region.

Thermokarst lakes are hotspots of CH_4 emissions (Schuur et al., 2022). On the TP, thermokarst lakes have shown significant spatial variations in CH_4 emissions, ranging from 0.02 to 1680 mg C m^{-2} d^{-1} (average of 110.4 mg C m^{-2} d^{-1}), with the highest emissions in alpine meadows (Wang et al., 2021b). A recent study on TP 163 thermokarst lakes from May to October indicates carbon emissions are 45 mg C-CH_4 m^{-2} d^{-1} and 392.4 mg C-CO_2 m^{-2} d^{-1}, respectively (Mu et al., 2023). Current thermokarst lakes cover an approximate area of 2825.45 ± 5.75 km^2 based on the random forest model and manual visual vectorization methods that extracted thaw lake boundaries on the TP based on Sentinel-2 images (Wei et al., 2021c). Therefore, the total CH_4 emissions are estimated to be approximately 0.03–0.06 Gg C yr^{-1}, while the total CO_2 emissions from TP thermokarst lakes is estimated to be about 0.22 Gg C yr^{-1} (Text SI and Table S2). Despite their importance in climate change, current estimates of thermokarst lake CH_4 and CO_2 emissions are highly uncertain. Nevertheless, this permafrost carbon-climate feedback, to some extent, may accelerate climate warming (Koven et al., 2011; Natali et al., 2021; Vonk and Gustafsson, 2013).

2.4. Human impacts on permafrost carbon

Population growth on the TP in recent decades has exerted tremendous pressure on fragile alpine ecosystems, leading to local grassland degradation in the Three-River-Source region and Qilian Mountains (Wei et al., 2020). Therefore, ecological protection and construction projects have been deployed across the Tibetan Autonomous Region, Three-River-Source Region, Qilian Mountains, Hengduan Mountains and Gannan-Zoige Ecological Reserves. These projects include forest protection and construction, grassland protection and construction, water and soil erosion control, and desertification land management. These projects can be classified into three stages, namely exploration (1989–2003), rapid growth (2004–2014), and comprehensive development (2015 − present). By conducting massive ecological projects, the TP is becoming one of the largest ecological projects implemented in a single natural geographical unit in China and even the world.

Ecological restoration projects may directly (like CO_2 and CH_4 uptakes) and indirectly (cool soil temperature and reduce lateral carbon loss) affect permafrost carbon storage. Grassland restoration on the TP can significantly increase CO_2 sinks by 40%–60% (Liu et al., 2021). However, the duration of ecological restoration matters, given that its positive effect is saturated approximately 5–8 years after restoration. Alpine meadows and steppes are considerable CH_4 sinks (Wei et al., 2015), and grassland restoration promotes CH_4 uptake by approximately 20% via increasing soil permeability and reducing available nitrogen (Wei et al., 2012). Alpine wetlands are generally weak sources of CH_4, and wetland restoration would reduce CH_4 emissions by >50% via increasing vascular plant transport and oxidation. Ecosystem restoration may also affect soil thermal regime by enhancing evapotranspiration (Miehe et al., 2019; Shen et al., 2015), i.e., grassland restoration

significantly reduces soil temperature (0.3–2 °C) and increases soil moisture content (1%–4%), which would benefit permafrost carbon storage.

3. Glacier melting enhanced carbon release

Glaciers can store organic and inorganic carbon from local and distant sources (Hood et al., 2015). Under climate warming, most TP glaciers are losing mass at an unprecedented rate (Miles et al., 2021; Yao et al., 2022). The most significant glacier mass loss has occurred in the Tienshan, Himalayas, and Nyainqengtanglha Mountains, whereas glaciers in the Pamir, Karakoram, and western Kunlun Mountains have remained stable over recent decades (Farinotti et al., 2020; Yao et al., 2012). Glacial shrinkage has resulted in regional environmental impacts and biogeochemical responses (Chen et al., 2022; Nie et al., 2021; Yao et al., 2022). In particular, melting glaciers have caused changes in carbon status through runoff transport to the hydrosphere and GHG emissions to the atmosphere.

3.1. Carbon storage from TP glaciers

The TP hosts the most significant number of glaciers and most significant ice volume outside the polar regions ($7.02 \pm 1.82 \times 10^3$ km^3) outside the polar regions (Farinotti et al., 2019; RGI, 2017). The distribution of the TP glacier ice storage volume indicates that the ice volume in Karakoram (~2130 km^3) is greater than that in the Himalayas (~1200 km^3) (Farinotti et al., 2019). Other concentrated glacier ice volumes are distributed in Hindu-Kush/Pamir (987 km^3), Kunlun (784 km^3), Tienshan (750 km^3), and Nyainqengtanglha (405 km^3) (Fig. S2 and Table S3). In the inner TP, glaciers are primarily distributed in the Qiangtang Plateau region (including the Tanggula and Qilian Mountains), with an ice volume of 854 km^3 (Miles et al., 2021).

Previous studies have reported the current BC, POC, and DOC concentrations in glaciers across the TP (Kang et al., 2019; Kang et al., 2022; Li et al., 2018b; Li et al., 2021b; Zhang et al., 2017a; Zhang et al., 2017b). The average BC and POC concentrations of the glaciers are significantly higher in aged snow than that in snow pits and fresh snow (Fig. S3; Table S4) (Kang et al., 2022). The average BC concentrations in glacial snow and ice range from several to thousands of nanograms per gram (ng g^{-1}), with marked differences between glaciers. The DOC concentrations in surface snow are usually lower than those in snow pits or fresh snow (without the impact of the post-deposition process) (Niu et al., 2018). This is because DOC in surface snow usually undergoes scavenging or leaching, especially in the ablation zone, which cannot represent the original status when carbon deposited on the glaciers. Therefore, in this study, we used carbon data from snow pits or fresh snow as the average concentration to estimate the carbon storage. Meanwhile, ice core BC records indicate that BC concentrations have

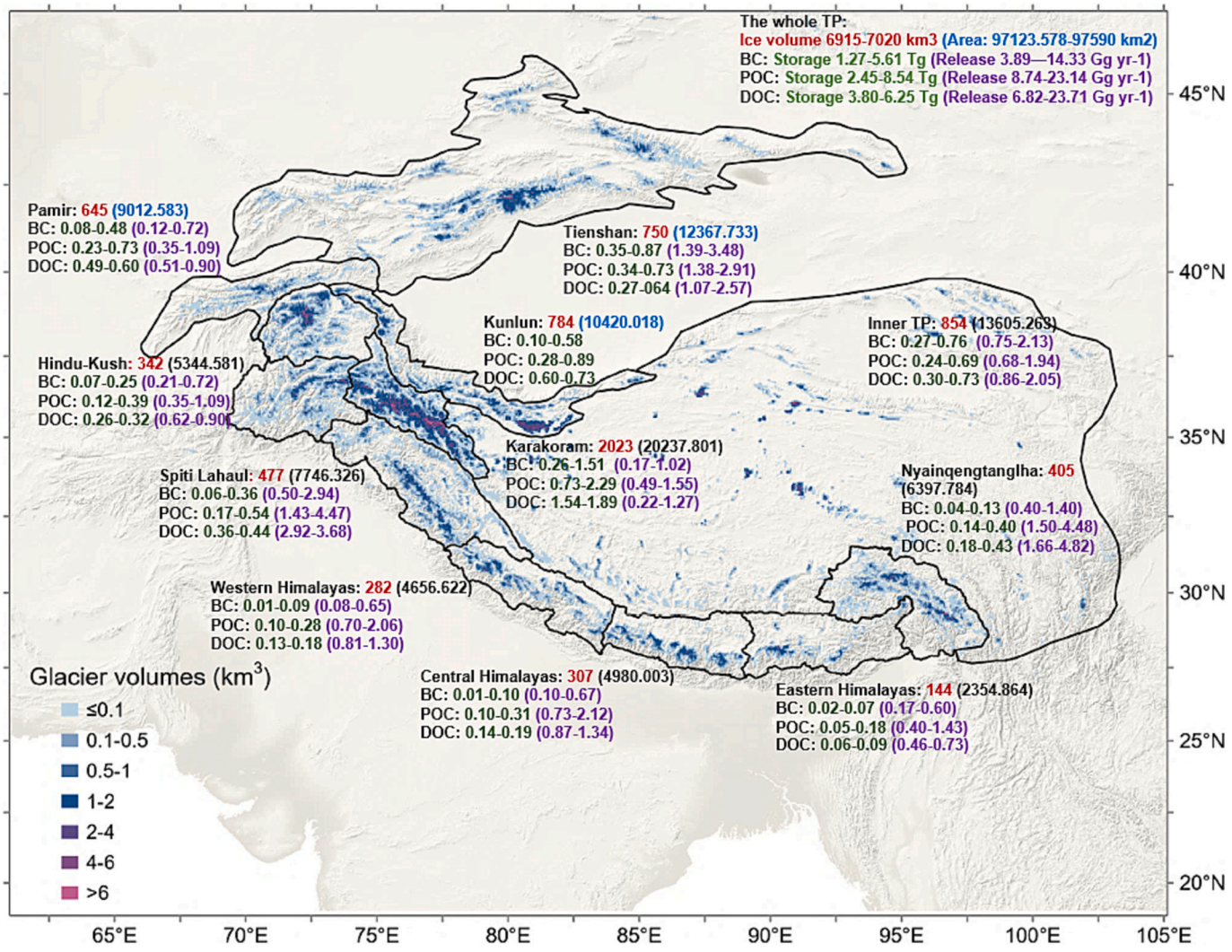

Fig. 4. Carbon storage and release from glaciers in subregions across the Third Pole. (Refer to Table S5 in *SI* for the glacier ice volume data and glacier mass balance data. See Text S2 in *SI* for the calculated carbon storage and release data.)

increased approximately three-fold from 1840 to 1940 (Kaspari et al., 2011; Wang et al., 2021d). Therefore, the minimum estimation was based on carbon data before the 1950s (three-fold lower than the current carbon concentrations), when anthropogenic activities played a minor impact on carbon emissions.

Based on glacier volume and carbon concentrations (Brun et al., 2018; Farinotti et al., 2019; Kang et al., 2022; Miles et al., 2021) (Text S2 and Table S4), the carbon storage of glaciers on the TP has been estimated (Fig. 4). The results indicate that the storage of BC, POC, and DOC for the entire TP is 1.27–5.61, 2.45–8.54, and 3.80–6.25 Tg, respectively, with higher storage in the Karakoram and Kunlun Mountains, mainly owing to the large glacier ice volume. The results also provide estimation of carbon storage in different subregions (Fig. 4 and Table S5). Our estimate of DOC storage in TP glaciers is comparable to previous studies (3.96 Tg C, (Liu et al., 2016)) but lower than estimates by Li et al. (2018b), with an estimate of 8.8–13.8 Tg C. Approximately 35% of the glaciers across the TP are highly unhealthy and expected to lose at least half their volume by 2100 without additional climate warming (Miles et al., 2021). The decline of ice volume will substantially decrease the carbon storage. The most significant reduction of carbon storage will occur in the Himalayan and Nyainqengtanglha Mountains, with the larger glacier mass loss in these regions.

3.2. Carbon release due to glacier mass loss

Glacier melting leads to carbon release through glacial runoff. Previous studies revealed an accelerating rate of glacier mass loss across the entire TP (Yao et al., 2012), which has been estimated to be approximately -16.3 ± 3.5 Gt yr^{-1} between 2000 and 2016 (Brun et al., 2017), -19.0 ± 2.5 Gt yr^{-1} between 2000 and 2018 (Shean et al., 2020), and -21.1 ± 4.8 Gt yr^{-1} between 2000 and 2019 (Hugonnet et al., 2021). The total glacier mass loss from 2000 to 2018 was approximately 340 Gt (Yao et al., 2022). For different subregions, the glacier mass balance shows a more significant deceleration in the Himalayan and Nyainqentanglha Mountains (Fig. S4) (Brun et al., 2017; Miles et al., 2021), with glacier mass lost at a rate of 0.37–0.40 m yr^{-1} during the past two decades.

Carbon release into downstream freshwater ecosystems is difficult to constrain. Previous studies estimated that glacier-stored DOC was approximately 3.96 Tg C in Chinese glaciers (Liu et al., 2016), with a glacially derived DOC release of 12.7–13.2 Gg C yr^{-1} from the TP and 15.4C yr^{-1} from the Chinese Territory (Liu et al., 2016; Yan et al., 2016). For Asian mountain glaciers, the estimates of storage and associated release of DOC are 8.8 to 13.8 Tg C and 0.19 Tg C yr^{-1}, respectively (Li et al., 2018b). Combining the average BC, POC, and DOC concentrations from glaciers with the glacier mass loss data (Tables S2 and S3), the release rate of BC, POC, and DOC from glacial melting is estimated to be 3.89–14.33, 8.74–23.14, and 6.82–23.71 Gg yr^{-1}, respectively (Fig. 4; Table S5). During the past two decades, the total carbon release has been calculated to be 389–1224 Gg C.

3.3. GHG emissions from glacial basins

Glaciers on the TP contain large reservoirs of organic carbon that can influence glacial ecosystems under rapid melting (Li et al., 2018b). We estimated the lateral export of carbon from glaciers melting water, as described in the previous section. A preliminary study found that cryoconite holes on the surface of glaciers in the southern and southeastern regions of the TP are possibly strong sources of carbon with positive fluxes of CH_4 and CO_2 during the strong ablation season; however, cryoconite holes may constitute a weak sink of atmospheric CH_4, as evidenced by the observed flux at the Dongkedima glacier in the central TP (Zhang et al., 2021b). Without accurate information on the areas of cryoconite holes distributed on glaciers and systematic observations of GHG emissions from cryoconite holes in different seasons, we cannot quantify the actual emissions at current.

Glacier retreat has also led to the exposure of subglacial sediments. The observations have revealed that the CH_4 and CO_2 fluxes from subglacial sediments average to be approximately 0.06 mg C m^{-2} d^{-1} and 24.12 mg C m^{-2} d^{-1}, respectively, serving as a possible carbon source (Zhang et al., 2021b). Over the past two decades, glacial areas have decreased by approximately 15%, resulting in approximately 14,600 km^2 of subglacial sediment exposure (Guo et al., 2015; IPCC, 2019). As a result, the estimated CH_4 and CO_2 emissions from these subglacial sediments are approximately 0.42 Gg C yr^{-1}. However, this estimation has significant uncertainties because there are only four sites for measuring carbon emissions from subglacial sediments (Zhang et al., 2021b).

The measured CH_4 and CO_2 concentrations from proglacial river runoff in the northern TP demonstrate that meltwater is a source of CH_4 because the average saturation is over 100%. However, CO_2 saturations vary significantly; the CO_2 fluxes exhibit positive (released CO_2) or negative (absorbed CO_2) values because the water and atmospheric conditions are variable (Du et al., 2022). Another study found that the average value of the observed CH_4 flux from Tibetan river runoff is 26.7 mg C m^{-2} d^{-1}, indicating this as a significant source of CH_4 (Qu et al., 2017a). The CH_4 flux of Tibetan proglacial river runoff was significantly lower than that from Tibetan rivers (142.8 mg C m^{-2} d^{-1}) (Zhang et al., 2020), which also departs from the global range reported for river streams. Meanwhile, proglacial river runoff serves as a significant sink of atmospheric CO_2 (-155 mg C m^{-2} d^{-1}) (Zhang et al., 2021b). This may be due to the elevated chemical weathering rates (Li et al., 2022c), which will change the capacity of carbon sources or sinks in glacial basins.

Given current climate warming, we must further investigate and understand the impact of glacial shrinkage on CH_4 and CO_2 fluxes on the TP. Specifically, CH_4 and CO_2 fluxes from cryoconite holes, subglacial sediments, and proglacial rivers must be thoroughly investigated to enhance our understanding of the carbon cycle.

4. Carbon emissions from TP rivers

Headwater rivers are important inland waters on the TP and are critical for carbon transport and emissions, further impacting the regional carbon cycle (Chen et al., 2022). They are considered significant sources of carbon emissions (Lin et al., 2023; Xun et al., 2022; Zhang et al., 2020). Changes in glacier and snow melting, permafrost thawing, and divergent changes in the strength of the Westerlies and Indian monsoon have led to significant changes of river runoff on the TP (Yao et al., 2022). Rivers originating from the TP have exhibited widespread changes from 1980 to 2018, significantly affecting the hydrological processes and water supply capacity in key Asian basins (Li et al., 2022a; Nie et al., 2021). Recently, DOC and GHG field observation sites for rivers are mostly distributed in the eastern and southern TP (Fig. S5).

4.1. Riverine DOC transport

Riverine carbon transport can connect terrestrial, oceanic, and atmospheric carbon pools, which will influence global and regional carbon cycles (Raymond and Bauer, 2001; Raymond et al., 2013). The mean DOC yield of global rivers is approximately 1.08 g C m^{-2} yr^{-1} (Li et al., 2019a). Spatial and temporal variations in the riverine DOC fluxes have been examined in several rivers on the TP (Table S6). For the Yellow River, the mean annual concentrations of riverine DOC ranged from 2.03 to 2.34 mg C L^{-1} (average of 2.21 mg C L^{-1}), with the highest concentrations in spring and summer and the lowest in winter (You and Li, 2021). For the Yangtze River, riverine DOC concentrations ranged from 0.2 to 2.8 mg C L^{-1} with the highest concentrations in July and the lowest in October (You et al., 2022). In another study, DOC concentrations from the Yellow, Yangtze, Langcang, and Nu rivers are approximately 5.45, 6.79, 4.42, and 4.43 mg C L^{-1}, respectively (Zhang et al., 2020). The average DOC concentrations for the Yarlung Tsangpo and

Indus rivers are approximately 1.16 and 0.99 mg L^{-1}, respectively (Qu et al., 2017a; Qu et al., 2017b). For the Upper Heihe River in the northern TP, DOC concentrations range from 0.25 to 12.2 mg L^{-1} (average of 0.82 mg L^{-1}) (Gao et al., 2019). The average DOC yield of TP rivers is approximately 0.41 g C m^{-2} yr^{-1}, which is lower than most other rivers due to the low DOC concentrations (Qu et al., 2017b). Based on previous studies, we conclude that the average riverine DOC ranges from 0.82 to 6.79 mg C L^{-1}, which is lower than that reported from rivers in Sayan–Altai Mountain Region of Tyva (about 2–6 mg C L^{-1}) (Byzaakay et al., 2023). The annual discharge of the TP glacier runoff from the initially glacierized area is estimated to be approximately 169 $\times$ 10^9 m^3 from 2011 to 2020 (under RCP2.6) (Huss and Hock, 2018). Therefore, the total DOC transported by river runoff from the TP is calculated to be approximately 0.1378–1.1414 Tg C yr^{-1} (Table S8). In most rivers, riverine DOC is mainly derived from the surrounding terrestrial ecosystem (Hansell et al., 2004). SOC can be degraded into DOC via microbial activity and leached into streams and rivers through the soil water (Stanley et al., 2012). A positive correlation between the radiocarbon age and permafrost watershed coverage has been observed, indicating that ^{14}C depleted/old carbon is exported from the TP permafrost regions during periods of high flow (Qu et al., 2017b).

BC is also an essential component of the riverine carbon exported to the ocean (Coppola et al., 2022; Jaffe et al., 2013). Riverine BC can be divided into particulate and dissolved BC with different environmental transport mechanisms, residence times, and fates. The global riverine flux of BC accounts for 43 Tg C yr^{-1}, which is 4–32% of the global annual BC emissions (Coppola et al., 2022; Coppola et al., 2018). However, no related studies on riverine BC have been reported on the TP. Therefore, measurements of BC export rates from downstream TP rivers and quantification of their legacy BC sources are required to close the regional BC budget.

4.2. GHG emissions from TP rivers

Despite their role in transporting water and carbon from the terrestrial environment to the ocean, rivers play a major biogeochemical role in the global carbon cycle and act as hotspots for CO_2 and CH_4 emissions to the atmosphere (Raymond et al., 2013). Global rivers can emit approximately 6.6 Pg CO_2 yr^{-1} and 29.5 Tg CH_4 yr^{-1}, almost equivalent to the CO_2 emitted into the atmosphere (Li et al., 2021a). Furthermore, headwater rivers contribute to more than two−thirds of the GHGs emissions from global rivers, indicating that headwater rivers are an essential source of GHGs to the atmosphere (Li et al., 2021a).

Studies on the eastern and southern TP (Fig. S5) reveal that, most rivers are supersaturated with CO_2 and CH_4, with calculated fluxes of 3452 mg C m^{-2} d^{-1} and 26.7 mg C m^{-2} d^{-1}, respectively (Qu et al., 2017a) (Table S9 in *SI*). In the source region of the Yangtze River in the central TP, small headwater streams are CO_2 hot spots that show significantly higher CO_2 partial pressures (52% higher) and CO_2 fluxes (792% higher) than larger rivers (Song et al., 2023). In the northern TP (Qinghai Lake Basin), CH_4 concentrations in rivers range from 25 to 1239 nmol L^{-1}, with diffusion fluxes of 41.2–78.8 mg C m^{-2} d^{-1}; meanwhile, surface river water was super-saturated with CO_2 (average of 528.89 μatm), indicating a high diffusion flux of CO_2 during spring (2633 mg C m^{-2} d^{-1}) and low values during winter (693 mg C m^{-2} d^{-1}) (Lin et al., 2023). An up-scaled estimation based on third- to seventh-order waterways in the eastern TP indicates that TP river outgassing is approximately 1.27 Tg CH_4 yr^{-1} and 17.5 Tg CO_2 yr^{-1} (Zhang et al., 2020). These studies suggest that the TP rivers could be sources of GHGs for delivery to the atmosphere. Particularly in summer, high rainfall and more thaw-released water yield high discharges, which can increase the water velocity, gas exchange rate, and thus the carbon emissions flux (Song et al., 2023). A latest study in Central Asia (Sayan–Altai Mountain Region, Tyva) revealed that CO_2 emissions from the surface of rivers are quite low (50–150 mg C m^{-2} d^{-1}), and they are impacted by the complexity of the external and internal factors controlling the CO_2 exchange between water surfaces and the atmosphere (Byzaakay et al., 2023).

Global GHG measurements from rivers indicate that the concentrations of riverine GHGs decrease continually with increasing stream order (Li et al., 2021a). Headwater streams of the first- to third-order usually have low dissolved oxygen, massive terrestrial carbon and nitrogen inputs, and large gas exchange velocities, resulting in high GHG emissions (Li et al., 2021a). The ebullitive CH_4 fluxes from TP rivers decrease exponentially with increasing stream order, whereas diffusive fluxes decrease linearly; CO_2 fluxes decrease from third- to fifth-order streams but increase in sixth- and seventh-order rivers (Zhang et al., 2020). However, estimations of GHG emissions from TP rivers are lacking for Strahler stream orders of 1–3, which are significantly influenced by glacier and permafrost meltwater. GHG emission from proglacial runoff (first-order waterway) reveal that the average CO_2 flux is −155 mg C m^{-2} d^{-1} (Zhang et al., 2021b), indicating a possible sink of CO_2, contrary to the previous consumption. The CH_4 flux from proglacial river runoff in the TP is 0.10 mg C m^{-2} d^{-1}; however, in the Kuoqionggangri Glacier Basin (southern TP), the CH_4 flux is −0.41 mg C m^{-2} d^{-1} (Zhang et al., 2021b). Limited data on GHGs from rivers directly affected by glacier melting and permafrost thawing have hampered our discussion on emissions associated with the stream orders, which yields significant uncertainties in estimating the total GHG emissions from rivers. The divergent variations in GHG emissions from proglacial river runoff and their causes require further investigation.

5. GHG emissions from TP lakes

Lakes are also essential inland waters and critical sources of GHG emissions (Sanches et al., 2019; Zheng et al., 2022). Earlier studies estimate that CH_4 emissions from lakes are 8–48 Tg, accounting for approximately 6–16% of global natural emissions (Bastviken et al., 2011). In Chinese lakes and reservoirs, a study has revealed diffusive emissions of 1.56 Tg C − CH_4 yr^{-1} and 25.2 Tg C − CO_2 yr^{-1}, with the highest GHGs emissions from TP lakes (Li et al., 2018a). On the TP, the number and area of lakes have increased from 1080 to 1424 and from 40,124 to 50,323 km^2 during 1976–2018, respectively (Zhang et al., 2019). These changes can substantially affect regional carbon cycles. In the northern TP (Fig. S5, Table S7 in *SI*), the fluxes of CO_2 and CH_4 in the Qinghai and Hala lakes range from −15.48 to −62.88 and 0.07 to 0.42 mg C m^{-2} d^{-1}, respectively, indicating that high-altitude lakes act as sinks of CO_2 (Wang et al., 2022a). On the southern TP, the fluxes of CO_2 in freshwater lakes (approximately −93.3 mg C m^{-2} d^{-1}) are significantly lower than that in brackish lakes (approximately 197 mg C m^{-2} d^{-1}) (Wen et al., 2017). The CH_4 flux at the water−air interface in freshwater lakes (0.54 mg C·m^{-2}·s^{-1}) is 15 − fold higher than that in brackish lakes (0.04 mg C·m^{-2}·s^{-1}) (Xun et al., 2022). The average diffusive fluxes of CO_2 and CH_4 from lakes across the eastern and southern TP are 884 and 62.4 mg C m^{-2} d^{-1}, respectively (Yan et al., 2018). Usually, permafrost thawing exerts the largest impact on lake water hydrochemistry and carbon pattern including CO2 exchange with the atmosphere (Byzaakay et al., 2023). Besides, salinity is another important factor regulating lake GHGs. The results indicated that, with salinity gradients across lakes, CO_2 flux enhancement could be compensated for by decrease in diffusive CH_4 flux at the water-air interface (Xun et al., 2022).

The lake area on the TP is approximately 50,323 km^2 in 2018 (Zhang et al., 2019). Most lakes on the TP have significant temporal variations in CO_2 release during different periods, such as the ice-free, freeze, fully frozen and thawed periods in Qinghai Lake (Li et al., 2022b). The general CH_4 fluxes range from 0.07 to 62.88 mg C m^{-2} d^{-1} (Table S10 in *SI*). The number of free-ice days per year is approximately 200 days. Then the estimated annual CH_4 emissions are approximately 0.66–633 Gg C yr^{-1}, averaged to approximately 211 Gg C yr^{-1}. Therefore, CO_2 emissions are estimated to be approximately 1.565 Tg C yr^{-1}. However, these measured fluxes lack winter observations, resulting in estimations with

significant uncertainties. Meanwhile, even for the same lake, CO_2 flux measurements fluctuate significantly (Wang et al., 2022a). Therefore, we must strengthen long-term high-resolution observations of lake GHG emissions.

6. Impacts of TP cryospheric and hydrospheric changes on carbon dynamics

6.1. Contributions of cryospheric and hydrospheric changes to TP carbon balance

In the "Global Carbon Budget 2022" (Friedlingstein et al., 2022) and "Global Methane Budget 2000−2017" (Saunois et al., 2020), few estimations have discussed the coupling impact of cryospheric and hydrospheric changes, except for the permafrost (IPCC, 2021). Recently, ice sheets export high rates of CH_4 into the atmosphere, which should be considered in the CH_4 budget (Lamarche-Gagnon et al., 2019; Wadham et al., 2012). Previous studies have also estimated carbon stocks in the water, biomass, and soil of different ecosystems (Chen et al., 2022). However, knowledge of the links between cryospheric and hydrospheric changes and carbon variability across the TP is still lacking. Fig. 5 summarizes carbon storage and release related to changes in the cryosphere and hydrosphere over the TP. Changes in the cryosphere and carbon cycle are complete and cannot be separated. In particular, the impact of glacier and permafrost ablation on carbon loss and emissions under continued climate warming cannot be ignored.

In recent decades, the TP glaciers have experienced rapid retreat (Farinotti et al., 2019; Miles et al., 2021; Yao et al., 2012). The observed glacier mass balance has shown a continuous negative trend since the mid-1990s (Zhang et al., 2021a). For instance, the glacier mass balance of Xiaodongkemdi Glacier in the central TP and Urumqi Glacier No. 1 in Tienshan was positive until the early 1990s and subsequently increased negative over time (Yao et al., 2012; Zhang et al., 2021a). This decreasing trend is projected to continue until the year of 2100 (IPCC, 2019). The total glacier mass loss over the TP from 2000 to 2018 was estimated to be approximately 340 Gt (Yao et al., 2022), which influences the seasonality and total discharge of river runoff (Immerzeel et al., 2010). Glacier melting also contributes to carbon loss from legacy carbon stored in glaciers (Li et al., 2018b). Our estimated results indicate that TP glacier melting contributed to the lateral carbon loss of 0.37–1.16 Tg during 2000–2018 based on the annual release rates of BC, POC, and DOC. Melting glaciers on the TP are a potential source of carbon-related GHGs (Zhang et al., 2021b). Meanwhile, the total TP glacial runoff is likely to reach its peak water between 2029 and 2056 under different RCP climate scenarios (Huss and Hock, 2018; Zhao et al., 2023).

Consequently, the number and area of glacial lakes in the TP are growing rapidly owing to climate arming, glacier retreat and permafrost thawing (IPCC, 2019; Zhang et al., 2022). The latest study reported the GHG emissions from several TP glacial lakes with CH_4 emission range of 0.05–49.0 mg C m^{-2} d^{-1}; whereas the daily average CO_2 flux was −61.2 mg C m^{-2} d^{-1}, and the CO_2 consumption could reach 38.9 Gg C yr^{-1} by all glacial lakes in the TP (Yan et al., 2023). However, it is still difficult to systematically estimate GHG emissions through the entire TP glacial lakes owing to limited observation data. Therefore, the impact of glacier shrinkage on CH_4 and CO_2 fluxes in this region requires further investigation. In particular, we must address, in detail, the CH_4 and CO_2 fluxes from cryoconite holes, subglacial sediments, proglacial rivers, and glacial lakes.

Widespread permafrost thawing is projected to occur by 2100, releasing tens to hundreds of billions of tons of permafrost carbon as CO_2 and CH_4 into the atmosphere, further exacerbating climate change (IPCC, 2019). Permafrost degradation, especially thermokarst, will hasten carbon emissions. Observations of carbon release from thermokarst lakes or permafrost collapses over the TP still remain sparse. Previous studies have revealed carbon loss from permafrost degradation through the lateral loss of SOC or GHG emissions to the atmosphere (Gao et al., 2021b; Mu et al., 2020). Permafrost carbon cycling and its climate

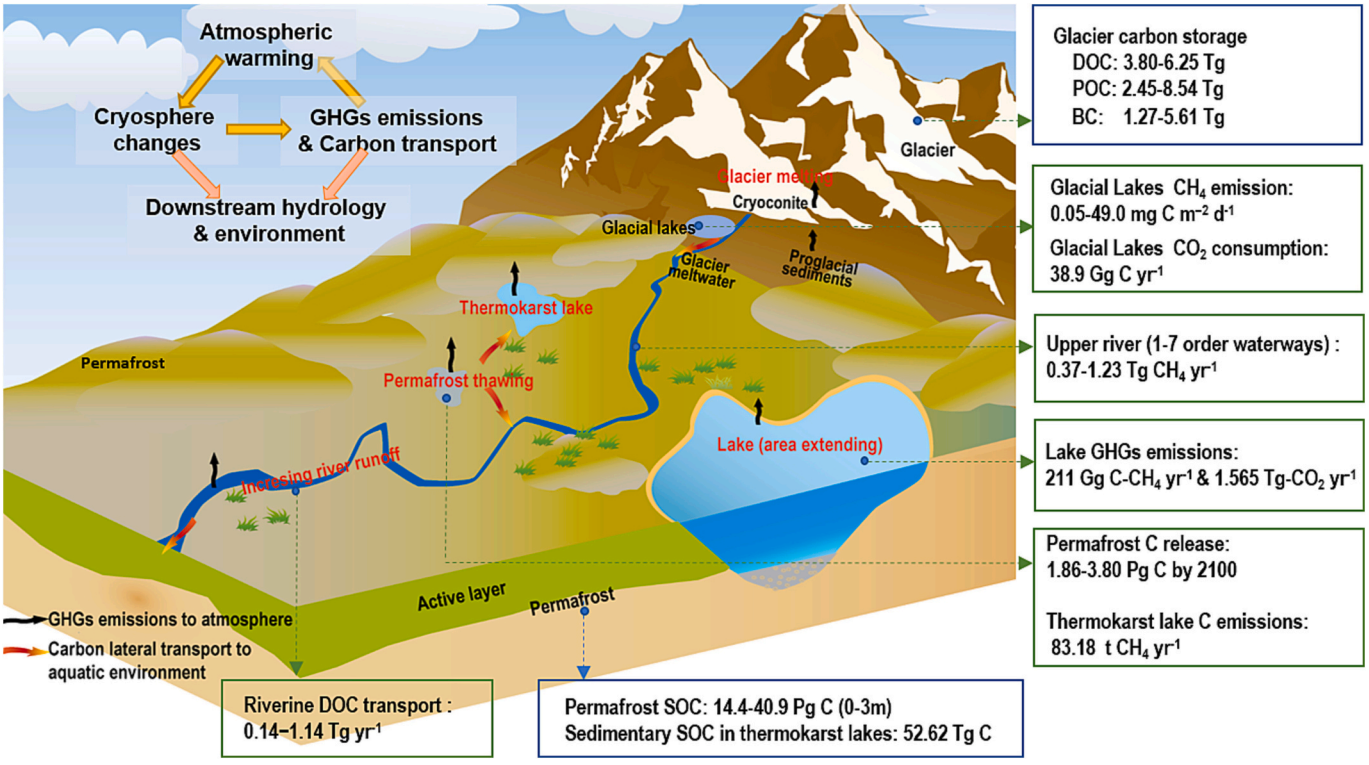

Fig. 5. A summary of cryospheric and hydrospheric changes and carbon release and transport over the Third Pole region. The storage and release data are summarized and calculated in this study.

feedback are essential foci of research on global change. The need for more sufficient knowledge of the critical process of permafrost carbon cycling (e.g., active layer dynamics and thermokarst erosion) has impeded any consensus on permafrost carbon feedback (Ding et al., 2022). Establishing systematic observations and effective projections requires an accurate estimation of emissions.

As important inland waters, rivers and lakes on the TP are also affected by glacier melting and permafrost degradation. The synthesized observations and model projections showed that accelerated transformations of snow and ice core into liquid water on the TP has resulted in changes in river runoff and lake expansion (Yao et al., 2022),with water gains in endorheic basins and water losses in exorheic basins. (Chen et al., 2022) also pointed out that changing hydrology and landscapes can directly or indirectly alter regional carbon cycle. Understanding how cryospheric-related changes affect the hydrosphere and water quality and their related carbon emissions requires more detailed monitoring networks.

6.2. *Carbon release from glacier cryoconite holes and thermokarst lakes*

Cryoconite holes (Fig. 6) are small water bodies formed when dark organic and inorganic debris attaches to glacier ice surfaces and consequently decreases the local albedo. They play essential roles in glacier mass balance, glacial geochemistry, and carbon cycling (Anesio et al., 2009; Bellas et al., 2020; Cook et al., 2016; Fountain and Tranter, 2008). They are mostly perennially ice-lidded and unique ecosystems on glaciers with abundant mineral and organic components that can form biological consortia with archaea, algae, cyanobacteria, fungi, and heterotrophic bacteria (Cook et al., 2016; Hodson et al., 2008). Cryoconite holes usually experience nutrient limitation at near-freezing temperatures and possess a highly truncated food chain (Sawstrom et al., 2002). The morphological characteristics of cryoconite vary significantly among different glaciers, which may be caused by differences in the sizes and types of inorganic mineral particles, as well as the types of cyanobacteria and other microorganisms (Cook et al., 2016; Liu et al., 2017). However, few studies have examined cryoconite formation process. In the Yushugou Glacier cryoconite of Tienshan, a study revealed that the organic (blue–green algae and organic matter) and inorganic (inorganic mineral particles) components combine to form a spherical polymer (likely a biofilm), indicating that its growth varies seasonally and has an alternative cycle of growth and decomposition (Xu et al., 2014).

Glacier microorganisms are widely involved in the biogeochemical cycles of glacial ecosystems and are the main drivers of the regional carbon cycle (Liu et al., 2022b). Cryoconite bacterial communities are dominated by Cyanobacteria, Chloroflexi, Betaproteobacteria, Bacteroidetes, and Actinobacteria, which vary by geographical location and exhibit significant differences among glaciers (Liu et al., 2017). For riverbed sediments on the TP (Zhang et al., 2020), approximately 48.5% of the sequences were methanogens, exhibiting a close phylogenetic relationship with the psychrotolerant species of Methanomicrobiales detected in glacial habitats in the polar regions (Boetius et al., 2015). A relatively high methanogen *mcrA* gene abundance in alpine waterways on the TP (8.1×10^4 copies per gram of dry sediment on average) indicates a great microbial potential for net CH_4 production (Zhang et al., 2020).

Globally, the percentage of organic matter in cryoconite samples ranges from 1.8% to 18.3% (Cook et al., 2016). The total OC content in cryoconites in TP glaciers varies from 0.1 (Muztag glacier in west TP) to 6.7% (Yulong Snow Mountain in southeastern TP), with higher values in the southeastern TP (Li et al., 2019b). Measurements of the cryoconite holes yielded CH_4 fluxes of 7.25 and 2.79 μmol m^{-2} d^{-1} in the melting season in the southeastern and northern TP, respectively (Zhang et al., 2021b). We also found that when the bubbles on the cryoconite holes break, the CH_4 and CO_2 concentrations rapidly increase by approximately 20 ppbv and 5 ppmv, respectively (Zhang et al., 2021b). Therefore, cryoconites may play a complex yet uncertain role in supraglacial climate processes. However, the ability to constrain GHG emissions with the function of the methanogen *mcrA* gene abundance and OC concentrations from cryoconite holes remains unclear. The

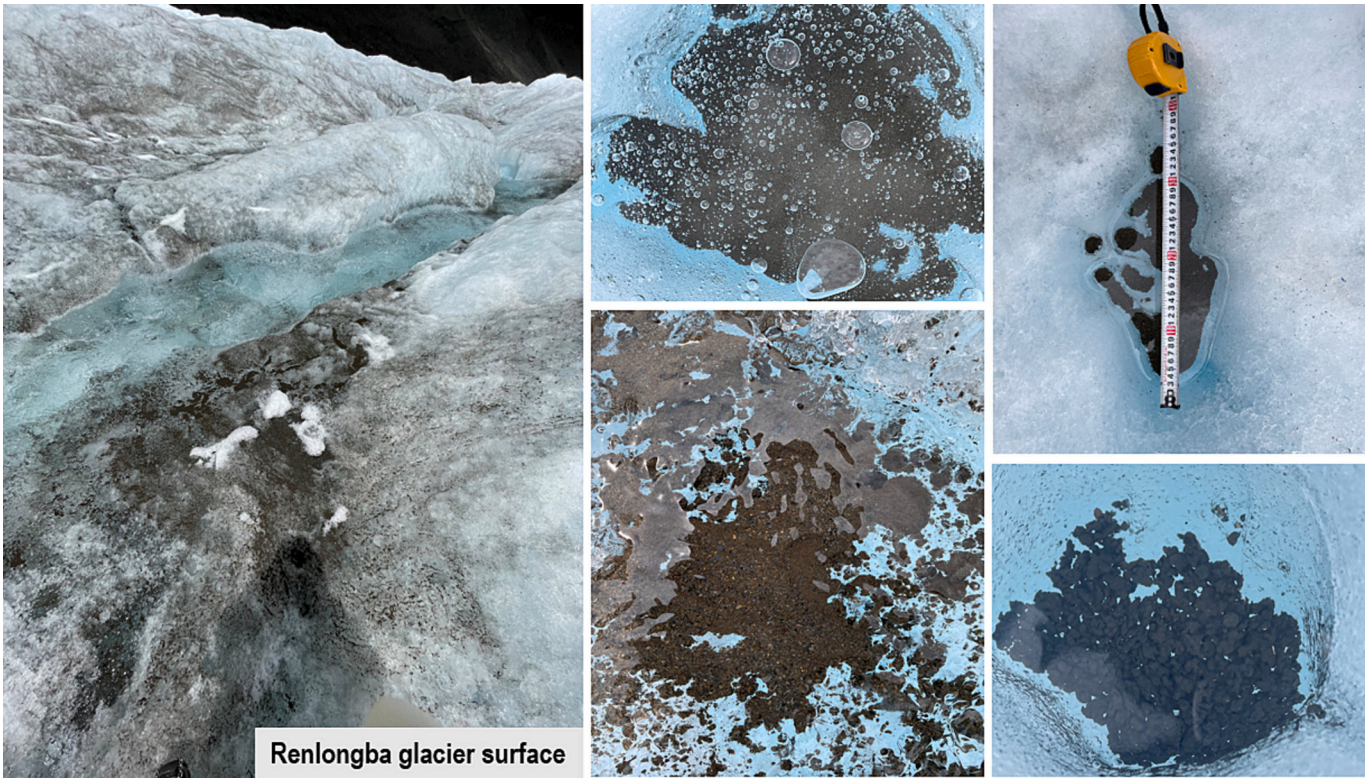

Fig. 6. Cryoconite distributed on the Renlongba glacier in southeast Tibet. (photos by Yulan Zhang).

effects of morphological characteristics and the cryoconite formation process on CH_4 emissions require careful investigations. Quantifying CH_4 emission pathways and their production from cryoconite holes will improve our understanding of the response of CH_4 emissions over the TP to climate change.

GHG emissions, particularly CH_4 emissions from thermokarst lakes, have been analyzed over the Arctic regions. Typically, thermokarst lakes are supersaturated in CO_2 and CH_4 in west Siberia; diffusive and ebullition emissions are the main pathways of CH_4 emitted to the atmosphere (Serikova et al., 2019). Groundwater discharge and lake drainage are also important drivers of CH_4 emissions from the Arctic lakes (Olid et al., 2022). On the TP, high methane emissions from thermokarst lakes are primarily attributed to ebullition fluxes (Wang et al., 2021b). However, previous studies have not addressed the relationship between the physiochemical variables of sediment and CH_4 production under different temperatures and vegetation types. A latest study reveals thermokarst lake sediment microbial abundance and hydrochemistry explain 51.9% and 38.3% of the total variance in CH_4 diffusive emissions (Mu et al., 2023). The characteristics of methanogens in sediments and their functions in CH_4 production must be illustrated in detail. There are several complex interactions between the biology and chemistry of permafrost lake sediments. However, their interactions with climate and anthropogenic pollutants remain a limitation of the current state of science.

6.3. *Climate response of carbon emissions to changing cryosphere and hydrosphere*

The IPCC AR6 has comprehensively illustrated the new understanding of the permafrost carbon cycle and its feedback to climatic warming (IPCC, 2021). In Arctic permafrost regions, the nonlinear process of abrupt permafrost thawing can increase carbon emissions 2–4 fold (Natali et al., 2021). Carbon emissions from permafrost thawing may exacerbate climate change (IPCC, 2021; Koven et al., 2011; Schuur et al., 2015).

As illustrated in Fig. 7, the possible interactions between cryosphere and hydrosphere changes and carbon dynamics on the TP is described. Accompanying rapid climate warming (You et al., 2021), the TP cryosphere is predicted to continuously retreat (Huss and Hock, 2018; Yao et al., 2022; Zhao et al., 2023), further changing the hydrosphere. Recently, the distribution and frequency of thermokarst lakes and retrogressive thaw slumps across the TP have been reported based on high-resolution satellite image interpretations and global position system (Gao et al., 2021b; Luo et al., 2022; Wei et al., 2021b). Based on findings of many studies across the TP, thawing permafrost has significantly increased carbon loss (Gao et al., 2021b; Mu et al., 2016; Wang et al., 2021b; Yang et al., 2018). However, the estimation of GHG emissions at the regional scale still needs to be improved for simulation, mainly because of the diversity of GHG sources in permafrost regions, including thermokarst lakes, ponds, and collapses. In particular, the thermokarst landscape can expose deep permafrost, accelerate thawing and amplify carbon emissions from the permafrost. However, with sufficient consideration of key permafrost and glacier carbon processes and observational data constraints, predictions of the feedback between the cryospheric carbon cycle, climate, and the relative contributions of CO_2 and CH_4 are more reliable than those of the TP.

Increased temperature and changing precipitation further enhance hydrological connectivity between glaciers, permafrost, and aquatic ecosystems (Yao et al., 2022). The warming rate on the TP was approximately 0.42 °C per decade during 1980–2018, almost twice the global average (Yao et al., 2022). Global warming has increased glacier melting, altering hydrological processes in the primary source regions of 13 major river systems and 1424 lakes with an area larger than 1 km^2 in Asia (Zhang et al., 2019). The projected increase in precipitation during the warm season (May to October) yields a total lake expansion of approximately 8000 and 9000 km^2 from 2015 to 2050 under scenarios SSP2–4.5 and SSP5–8.5, respectively (Liu and Chen, 2022). As a result, the lake area of Yamzhog Yumco (including Kongmu Co) will expand under all three scenarios (RCP2.6, RCP4.5, and RCP8.5) for three periods (short-term during 2016–2035, medium term during 2046–2065, and long term during 2081–2100) (Sun et al., 2021). Meanwhile, the rising temperature in the cold season (November to April of the following year) would lead to a decrease in the TP lake ice duration by 22 and 29 d by 2050s (35 and 71 days by 2100 s) under SSP2–4.5 and SSP5–8.5, respectively (Liu and Chen, 2022).

In addition, the total glacier runoff contributing to river runoff varies significantly from basin to basin and throughout the year over the TP. Peak water glacial runoff is expected to occur over two to three decades (Huss and Hock, 2018). It reveals that the peak water of 11 drainage basins on the TP will potentially occur before the 2050s, whereas the others will likely reach peak water between 2030 and 2080 (Zhao et al., 2023). During 1980–2018, the annual river runoff across most of the TP shows a significant increase in rivers (Yao et al., 2022). For example, mean annual runoff on the southeastern TP will increase by 11–13%

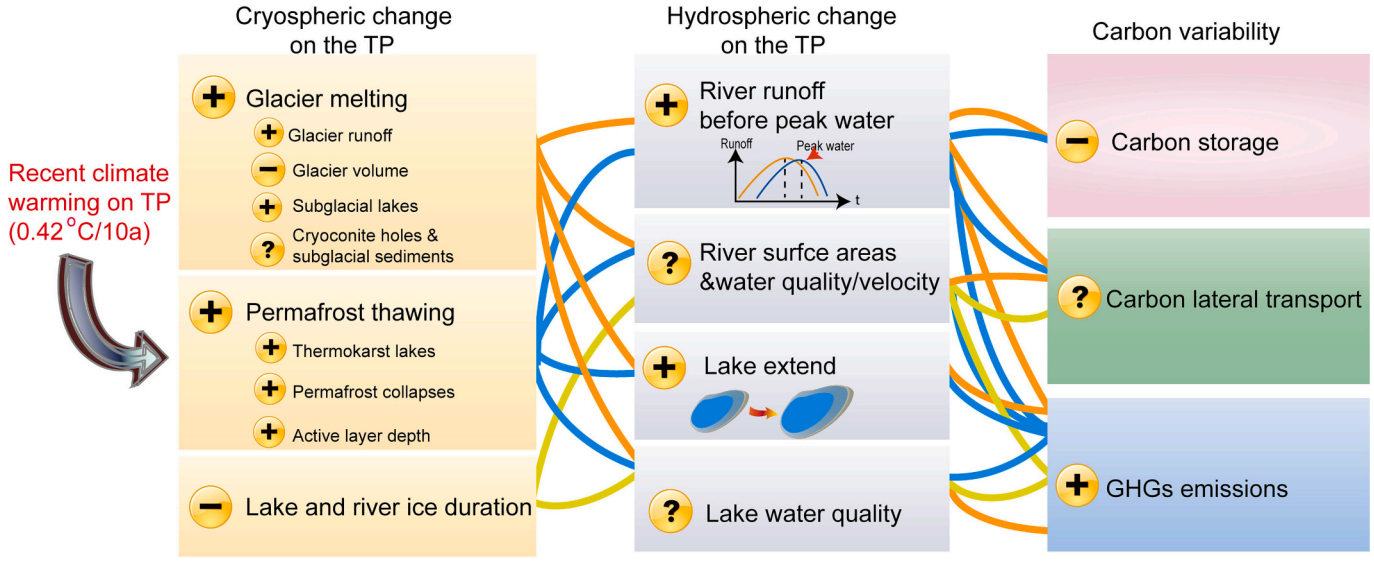

Fig. 7. Sketch map of interactions between cryosphere and hydrosphere changes and carbon dynamics on the Third Pole region under ongoing climate warming. The warming rate of 0.42 °C/10a during 1980–2018 across the TP cited from (Yao et al., 2022).

under a 1 °C increase in global mean air temperature (Li et al., 2013); The upper Indus River runoff will increase by 3.9 Gt per decade (Yao et al., 2022). However, river runoff has declined in the Yellow River (Yao et al., 2019). A previous study indicates that river discharge accounts for >95% of the annual CH_4 sea-to-air emissions from the estuary in Cambridge Bay, Canada (Manning et al., 2020). The freezing and melting of river ice is closely related to climate change, hydrology, and ecosystem conditions (Shiklomanov and Lammers, 2014). CH_4 concentrations in the river and ice-covered estuary reach up to 240,000% saturation and 19,000% saturation, respectively, but quickly drop by >100-fold flowing ice melt in Cambridge Bay (Manning et al., 2020). In the northern TP, the average area of river ice shows a weak decreasing trend from 1999 to 2018 and a negative trend with air temperature (Li et al., 2020a).

The rate of GHG fluxes and water surface areas play an essential role in total GHG emissions in the hydrosphere. DOC sequestered in glaciers and permafrost is primarily exposed and transported to the hydrosphere, converting dissolved carbon to CO_2 and CH_4 (Vonk et al., 2015), increasing CO_2 and CH_4 fluxes from the hydrosphere on the TP. Therefore, climate warming will significantly increase river runoff and lake extent, accelerating the CO_2 and CH_4 fluxes from the TP hydrosphere in the coming decades (Fig. 7). In addition, the impact of enhanced cryospheric melting on river and lake water quality and subsequently, the potential impacts on lateral carbon transport still need further investigated, especially in a warming climate.

7. Conclusions

The TP plays an essential role in water sustainability for a large proportion of the Asian population. However, marked climate warming in recent decades has caused cryosphere retreat and altered the hydrosphere and regional carbon cycles on the TP. Owing to its critical role in ecosystems and climate, the carbon cycle and dynamics on the TP have attracted significant attention. Based on a literature review, we provide an integrated understanding of cryospheric and hydrospheric changes and carbon cycling over the TP, highlighting carbon storage and release pathways from permafrost and glaciers. Estimating the carbon release from headwater rivers and lakes has also revealed the possible impact of cryospheric changes.

The synthesized analyses indicate that permafrost SOC stocks show an overall increasing trend from the southeast towards the northwest TP, with the most extensive SOC stocks in the wetland regions. The storage of SOC in the TP permafrost ranges from 15.3 to 40.9 Pg C at depths of 0–3 m based on different methods. Among the permafrost SOC, the contribution of POC is estimated to be approximately 6.34%. Sedimentary SOC from permafrost thaw lakes has been estimated to be 52.62 Tg C. Owing to abrupt permafrost thawing, approximately 23–37% of permafrost SOC has been removed and transported into aquatic environments (including rivers and lakes). Significant GHG emissions result from TP permafrost thawing. The estimated CH_4 emissions from permafrost thaw slumps and thermokarst lakes are 0.04–0.25 and 0.06 Gg C − CH_4 yr^{-1}, respectively.

For TP glaciers, the carbon storage of BC, POC, and DOC has been calculated to be 1.27–5.61, 2.45–8.54, and 3.80–6.25 Tg, respectively. Although carbon storage is less than that in permafrost, OC from glaciers is labile and tends to be released through lateral export or vertical GHG emissions. The estimated release of BC, POC, and DOC from glacier runoff was 3.89–14.33, 8.74–23.14, and 6.82–23.71Gg C yr^{-1}, respectively, with a total carbon loss of 389–1224 Gg C during the past two decades. GHG measurements in typical glacial basins on the TP revealed that cryoconite holes and subglacial sediments are strong GHG sources. GHG emissions from subglacial sediments are estimated to be approximately 0.42 Gg C yr^{-1}. Proglacial river runoff can also serve as a significant sink for atmospheric CO_2.

Cryospheric melting has also changed the regional water balance (hydrospheric changes), as evidenced by increasing river runoff and continuous lake extension, further influencing the regional carbon dynamics. On the TP, DOC transported by river runoff is calculated to be approximately 0.14–1.14 Tg yr^{-1}, serving as an essential link between carbon in the cryosphere and that in downstream regions. Riverine GHGs concentrations vary significantly among previous studies. An upscaled estimation indicates that TP river outgassing is approximately 1.27 Tg CH_4 yr^{-1} and 17.5 Tg CO_2 yr^{-1}. For TP lakes, the estimated annual CH_4 emissions are approximately 0.66–633 Gg C-CH_4 yr^{-1}, and CO_2 emissions are estimated to be approximately 1.565 Tg-CO_2 yr^{-1}. However, CH_4 and CO_2 fluxes from rivers and lakes lack extensive winter survey observations, which results estimation uncertainties.

The warming-induced melting of the cryosphere and changing hydrosphere, as well as their relationships with the carbon cycles on the TP, pose a challenge for ecosystem and climate projections. In particular, systematic observations, release pathways, and accurate estimations of GHG emissions from glaciers and lakes, rivers, permafrost thermokarst lakes, and collapses must be strengthened. Furthermore, we must constrain how the cryosphere interacts with other ecosystems (e.g., grasslands and wetlands) under climate warming. The study of molecular fingerprints in TP river systems might fill a gap and lead to better understanding of the processes responsible for the molecular transformation of natural organic matter across different landscapes, which can be considered a powerful instrument to identify distinct trends both in molecular composition and diversity of natural organic matter along large TP rivers.

The impact of the synergistic effects between cryospheric and hydrospheric changes and other pollutants (e.g., mercury) and how to accurately simulate and predict the climate and environmental impacts of carbon release under different climate change scenarios require further investigation. To achieve an integrated understanding of the role of the cryosphere in future carbon dynamics, we suggest building a framework that includes biogeochemistry, glaciology, hydrology, and climatic processes on the TP.

CRediT authorship contribution statement

Tanguang Gao: Conceptualization, Methodology, Writing – original draft. **Shichang Kang:** Writing – review & editing. **Tandong Yao:** Writing – review & editing. **Yanlong Zhao:** Software, Data curation. **Xuexue Shang:** Software, Data curation. **Yong Nie:** Writing – review & editing. **Rensheng Chen:** Writing – review & editing. **Igor Semiletov:** Writing – review & editing. **Taigang Zhang:** Software, Data curation. **Xi Luo:** Software, Data curation. **Da Wei:** Conceptualization, Supervision, Writing – review & editing. **Yulan Zhang:** Conceptualization, Supervision, Writing – review & editing.

Declaration of competing interest

The authors declare that they have no known competing financial interests or personal relationships that could have appeared to influence the work reported in this paper.

Data availability

Data will be made available on request.

Acknowledgements

This work was jointly supported by the Science and Technology Program of Gansu Province (23ZDFA017), the National Natural Science Foundation of China (42271132, 42322105), Outstanding Youth Fund of Gansu Province (23JRRA612), the West Light Scholar of the Chinese Academy of Sciences (xbzg-zdsys-202202), and the Youth Innovation Promotion Association of the Chinese Academy of Sciences (2020369).

Appendix A. Supplementary data

Supplementary data to this article can be found online at https://doi.org/10.1016/j.earscirev.2024.104717.

References

Abbott, B.W., Jones, J.B., 2015. Permafrost collapse alters soil carbon stocks, respiration, CH4, and N2O in upland tundra. Glob. Chang. Biol. 21 (12), 4570–4587.

Anesio, A.M., Hodson, A.J., Fritz, A., Psenner, R., Sattler, B., 2009. High microbial activity on glaciers: importance to the global carbon cycle. Glob. Chang. Biol. 15 (4), 955–960.

Anthony, K.M.W., Anthony, P., Grosse, G., Chanton, J., 2012. Geologic methane seeps along boundaries of Arctic permafrost thaw and melting glaciers. Nat. Geosci. 5 (6), 419–426.

Anthony, K.W., von Deimling, T.S., Nitze, I., Frolking, S., Emond, A., Daanen, R., Anthony, P., Lindgren, P., Jones, B., Grosse, G., 2018. 21st-century modeled permafrost carbon emissions accelerated by abrupt thaw beneath lakes. Nat. Commun. 9.

Azam, M.F., Kargel, J.S., Shea, J.M., Nepal, S., Haritashya, U.K., Srivastava, S., Maussion, F., Qazi, N., Chevallier, P., Dimri, A.P., Kulkarni, A.V., Cogley, J.G., Bahuguna, I., 2021. Glaciohydrology of the Himalaya-Karakoram. Science 373 (6557), 869-+.

Bastviken, D., Tranvik, L.J., Downing, J.A., Crill, P.M., Enrich-Prast, A., 2011. Freshwater methane emissions offset the continental carbon sink. Science 331 (6013), 50.

Bellas, C.M., Schroeder, D.C., Edwards, A., Barker, G., Anesio, A.M., 2020. Flexible genes establish widespread bacteriophage pan-genomes in cryoconite hole ecosystems. Nat. Commun. 11 (1).

Boetius, A., Anesio, A.M., Deming, J.W., Mikucki, J.A., Rapp, J.Z., 2015. Microbial ecology of the cryosphere: sea ice and glacial habitats. Nat. Rev. Microbiol. 13 (11), 677–690.

Brun, F., Berthier, E., Wagnon, P., Kaab, A., Treichler, D., 2017. A spatially resolved estimate of High Mountain Asia glacier mass balances from 2000 to 2016. Nat. Geosci. 10 (9), 668–+.

Brun, F., Berthier, E., Wagnon, P., Kaab, A., Treichler, D., 2018. A spatially resolved estimate of High Mountain Asia glacier mass balances from 2000 to 2016. Nat. Geosci. 10, 668–673.

Byzaakay, A.A., Kolesnichenko, L.G., Kolesnichenko, I.I., Khovalyg, A.O., Raudina, T.V., Prokushkin, A.S., Lushchaeva, I.V., Kvasnikova, Z.N., Vorobyev, S.N., Pokrovsky, O. S., Kirpotin, S., 2023. Dissolved Carbon Concentrations and Emission Fluxes in Rivers and Lakes of Central Asia (Sayan-Altai Mountain Region, Tyva). Water 15 (19).

Chen, L.Y., Liang, J.Y., Qin, S.Q., Liu, L., Fang, K., Xu, Y.P., Ding, J.Z., Li, F., Luo, Y.Q., Yang, Y.H., 2016. Determinants of carbon release from the active layer and permafrost deposits on the Tibetan Plateau. Nat. Commun. 7.

Chen, H., Ju, P.J., Zhu, Q., Xu, X.L., Wu, N., Gao, Y.H., Feng, X.J., Tian, J.Q., Niu, S.L., Zhang, Y.J., Peng, C.H., Wang, Y.F., 2022. Carbon and nitrogen cycling on the Qinghai-Tibetan Plateau. Nat. Rev. Earth Environ. 3 (10), 701–716.

Cook, J., Edwards, A., Takeuchi, N., Irvine-Fynn, T., 2016. Cryoconite: the dark biological secret of the cryosphere. Progr. Phys. Geogr. Earth Environ. 40 (1), 66–111.

Coppola, A.I., Wiedemeier, D.B., Galy, V., Haghipour, N., Hanke, U.M., Nascimento, G.S., Usman, M., Blattmann, T.M., Reisser, M., Freymond, C.V., Zhao, M.X., Voss, B., Wacker, L., Schefuss, E., Peucker-Ehrenbrink, B., Abiven, S., Schmidt, M.W.I., Eglinton, T.I., 2018. Global-scale evidence for the refractory nature of riverine black carbon. Nat. Geosci. 11 (8), 584–+.

Coppola, A.I., Wagner, S., Lennartz, S.T., Seidel, M., Ward, N.D., Dittmar, T., Santin, C., Jones, M.W., 2022. The black carbon cycle and its role in the Earth system. Nat. Rev. Earth Environ. 3 (8), 516–532.

Ding, J.Z., Wang, T., Piao, S.L., Smith, P., Zhang, G.L., Yan, Z.J., Ren, S., Liu, D., Wang, S. P., Chen, S.Y., Dai, F.Q., He, J.S., Li, Y.N., Liu, Y.W., Mao, J.F., Arain, A., Tian, H.Q., Shi, X.Y., Yang, Y.H., Zeng, N., Zhao, L., 2019. The paleoclimatic footprint in the soil carbon stock of the Tibetan permafrost region. Nat. Commun. 10.

Ding, J.Z., Wang, T., Wang, Y.Y., Chen, F.H., 2022. New understanding of the response of permafrost carbon cycling to climate warming. Sci. Bull. 67 (13), 1322–1325.

Du, Z.H., Wang, L., Wei, Z.Q., Liu, J.F., Lin, P.L., Lin, J.H., Li, Y.Z., Jin, Z.Z., Chen, J.Z., Wang, X.X., Qin, X., Xiao, C.D., 2022. CH4 and CO2 observations from a melting high mountain glacier, Laohugou Glacier No. 12. Adv. Clim. Chang. Res. 13 (1), 146–155.

Farinotti, D., Huss, M., Furst, J.J., Landmann, J., Machguth, H., Maussion, F., Pandit, A., 2019. A consensus estimate for the ice thickness distribution of all glaciers on Earth. Nat. Geosci. 12 (3), 168–+.

Farinotti, D., Immerzeel, W.W., de Kok, R.J., Quincey, D.J., Dehecq, A., 2020. Manifestations and mechanisms of the Karakoram glacier Anomaly. Nat. Geosci. 13 (1), 8–+.

Fountain, A.G., Tranter, M., 2008. Introduction to special section on Microcosms in Ice: the Biogeochemistry of Cryoconite Holes. J. Geophys. Res Biogeosci. 113 (G2).

Friedlingstein, P., Cox, P., Betts, R., Bopp, L., Von Bloh, W., Brovkin, V., Cadule, P., Doney, S., Eby, M., Fung, I., Bala, G., John, J., Jones, C., Joos, F., Kato, T., Kawamiya, M., Knorr, W., Lindsay, K., Matthews, H.D., Raddatz, T., Rayner, P., Reick, C., Roeckner, E., Schnitzler, K.G., Schnur, R., Strassmann, K., Weaver, A.J., Yoshikawa, C., Zeng, N., 2006. Climate-carbon cycle feedback analysis: results from the (CMIP)-M-4 model intercomparison. J. Clim. 19 (14), 3337–3353.

Friedlingstein, P., O'Sullivan, M., Jones, M.W., Andrew, R.M., Gregor, L., Hauck, J., Le Quere, C., Luijkx, I.T., Olsen, A., Peters, G.P., Peters, W., Pongratz, J., Schwingshackl, C., Sitch, S., Canadell, J.G., Ciais, P., Jackson, R.B., Alin, S.R., Alkama, R., Arneth, A., Arora, V.K., Bates, N.R., Becker, M., Bellouin, N., Bittig, H.C., Bopp, L., Chevallier, F., Chini, L.P., Cronin, M., Evans, W., Falk, S., Feely, R.A., Gasser, T., Gehlen, M., Gkritzalis, T., Gloege, L., Grassi, G., Gruber, N., Gurses, O., Harris, I., Hefner, M., Houghton, R.A., Hurtt, G.C., Iida, Y., Ilyina, T., Jain, A.K., Jersild, A., Kadono, K., Kato, E., Kennedy, D., Goldewijk, K.K., Knauer, J., Korsbakken, J.I., Landschutzer, P., Lefevre, N., Lindsay, K., Liu, J.J., Liu, Z., Marland, G., Mayot, N., McGrath, M.J., Metzl, N., Monacci, N.M., Munro, D.R., Nakaoka, S.I., Niwa, Y., O'Brien, K., Ono, T., Palmer, P.I., Pan, N.Q., Pierrot, D., Pocock, K., Poulter, B., Resplandy, L., Robertson, E., Rodenbeck, C., Rodriguez, C., Rosan, T.M., Schwinger, J., Seferian, R., Shutler, J.D., Skjelvan, I., Steinhoff, T., Sun, Q., Sutton, A.J., Sweeney, C., Takao, S., Tanhua, T., Tans, P.P., Tian, X.J., Tian, H.Q., Tilbrook, B., Tsujino, H., Tubiello, F., van der Werf, G.R., Walker, A.P., Wanninkhof, R., Whitehead, C., Wranne, A.W., Wright, R., Yuan, W.P., Yue, C., Yue, X., Zaehle, S., Zeng, J.Y., Zheng, B., 2022. Global Carbon Budget 2022. Earth Syst. Sci. Data 14 (11), 4811–4900.

Gao, T.G., Zhang, T.J., Guo, H., Hu, Y.T., Shang, J.G., Zhang, Y.L., 2018. Impacts of the active layer on runoff in an upland permafrost basin, northern Tibetan Plateau. PLoS One 13 (2).

Gao, T.G., Kang, S.C., Chen, R.S., Zhang, T.G., Zhang, T.J., Han, C.T., Tripathee, L., Sillanpaa, M., Zhang, Y.L., 2019. Riverine dissolved organic carbon and its optical properties in a permafrost region of the Upper Heihe River basin in the Northern Tibetan Plateau. Sci. Total Environ. 686, 370–381.

Gao, T.G., Wang, X.M., Wei, D., Wang, T., Liu, S.W., Zhang, Y.L., 2021a. Transboundary water scarcity under climate change. J. Hydrol. 598.

Gao, T.G., Zhang, Y.L., Kang, S.C., Abbott, B.W., Wang, X.M., Zhang, T.J., Yi, S.H., Gustafsson, O., 2021b. Accelerating permafrost collapse on the eastern Tibetan Plateau. Environ. Res. Lett. 16 (5).

Guo, W.Q., Liu, S.Y., Xu, L., Wu, L.Z., Shangguan, D.H., Yao, X.J., Wei, J.F., Bao, W.J., Yu, P.C., Liu, Q., Jiang, Z.L., 2015. The second Chinese glacier inventory: data, methods and results. J. Glaciol. 61 (226), 357–372.

Hansell, D.A., Kadko, D., Bates, N.R., 2004. Degradation of terrigenous dissolved organic carbon in the western Arctic Ocean. Science 304 (5672), 858–861.

Hodson, A., Anesio, A.M., Tranter, M., Fountain, A., Osborn, M., Priscu, J., Laybourn-Parry, J., Sattler, B., 2008. Glacial ecosystems. Ecol. Monogr. 78 (1), 41–67.

Hood, E., Battin, T.J., Fellman, J., O'Neel, S., Spencer, R.G.M., 2015. Storage and release of organic carbon from glaciers and ice sheets. Nat. Geosci. 8 (2), 91–96.

Hugelius, G., Strauss, J., Zubrzycki, S., Harden, J.W., Schuur, E.A.G., Ping, C.L., Schirrmeister, L., Grosse, G., Michaelson, G.J., Koven, C.D., O'Donnell, J.A., Elberling, B., Mishra, U., Camill, P., Yu, Z., Palmtag, J., Kuhry, P., 2014. Estimated stocks of circumpolar permafrost carbon with quantified uncertainty ranges and identified data gaps. Biogeosciences 11 (23), 6573–6593.

Hugonnet, R., McNabb, R., Berthier, E., Menounos, B., Nuth, C., Girod, L., Farinotti, D., Huss, M., Dussaillant, I., Brun, F., Kaab, A., 2021. Accelerated global glacier mass loss in the early twenty-first century. Nature 592 (7856), 726-+.

Huss, M., Hock, R., 2018. Global-scale hydrological response to future glacier mass loss. Nat. Clim. Chang. 8 (2), 135-+.

Immerzeel, W.W., van Beek, L.P.H., Bierkens, M.F.P., 2010. Climate Change Will Affect the Asian Water Towers. Science 328 (5984), 1382–1385.

Immerzeel, W.W., Lutz, A.F., Andrade, M., Bahl, A., Biemans, H., Bolch, T., Hyde, S., Brumby, S., Davies, B.J., Elmore, A.C., Emmer, A., Feng, M., Fernandez, A., Haritashya, U., Kargel, J.S., Koppes, M., Kraaijenbrink, P.D.A., Kulkarni, A.V., Mayewski, P.A., Nepal, S., Pacheco, P., Painter, T.H., Pellicciotti, F., Rajaram, H., Rupper, S., Sinisalo, A., Shrestha, A.B., Viviroli, D., Wada, Y., Xiao, C., Yao, T., Baillie, J.E.M., 2020. Importance and vulnerability of the world's water towers. Nature 577 (7790), 364-+.

IPCC, 2019. Summary for policymakers. In: IPCC Special Report on the Ocean and Cryosphere in a Changing Climate.

IPCC, 2021. Summary for policymakers. In: Climate Change 2021: The Physical Science Basis. Contribution of Working Group I to the Sixth Assessment Report of the Intergovernmental Panel on Climate Change.

Jaffe, R., Ding, Y., Niggemann, J., Vahatalo, A.V., Stubbins, A., Spencer, R.G.M., Campbell, J., Dittmar, T., 2013. Global charcoal mobilization from soils via dissolution and riverine transport to the oceans. Science 340 (6130), 345–347.

Jiang, L., Chen, H., Zhu, Q.A., Yang, Y.Z., Li, M.X., Peng, C.H., Zhu, D., He, Y.X., 2019. Assessment of frozen ground organic carbon pool on the Qinghai-Tibet Plateau. J. Soils Sediments 19 (1), 128–139.

Kang, S.C., Zhang, Q.G., Qian, Y., Ji, Z.M., Li, C.L., Cong, Z.Y., Zhang, Y.L., Guo, J.M., Du, W.T., Huang, J., You, Q.L., Panday, A.K., Rupakheti, M., Chen, D.L., Gustafsson, O., Thiemens, M.H., Qin, D.H., 2019. Linking atmospheric pollution to cryospheric change in the Third Pole region: current progress and future prospects. Natl. Sci. Rev. 6 (4), 796–809.

Kang, S.C., Zhang, Y.L., Chen, P.F., Guo, J.M., Zhang, Q.G., Cong, Z.Y., Kaspari, S., Tripathee, L., Gao, T.G., Niu, H.W., Zhong, X.Y., Chen, X.T., Hu, Z.F., Li, X.F., Li, Y., Neupane, B., Yan, F.P., Rupakheti, D., Gul, C., Zhang, W., Wu, G.M., Yang, L., Wang, Z.Q., Li, C.L., 2022. Black carbon and organic carbon dataset over the Third Pole. Earth Syst. Sci. Data 14 (2), 683–707.

Karlsson, J., Serikova, S., Vorobyev, S.N., Rocher-Ros, G., Denfeld, B., Pokrovsky, O.S., 2021. Carbon emission from Western Siberian inland waters. Nat. Commun. 12 (1).

Kaspari, S.D., Schwikowski, M., Gysel, M., Flanner, M.G., Kang, S., Hou, S., Mayewski, P. A., 2011. Recent increase in black carbon concentrations from a Mt. Everest ice core spanning 1860-2000 AD. Geophys. Res. Lett. 38.

Koven, C.D., Ringeval, B., Friedlingstein, P., Ciais, P., Cadule, P., Khvorostyanov, D., Krinner, G., Tarnocai, C., 2011. Permafrost carbon-climate feedbacks accelerate global warming. Proc. Natl. Acad. Sci. USA 108 (36), 14769–14774.
Lamarche-Gagnon, G., Wadham, J.L., Lollar, B.S., Arndt, S., Fietzek, P., Beaton, A.D., Tedstone, A.J., Telling, J., Bagshaw, E.A., Hawkings, J.R., Kohler, T.J., Zarsky, J.D., Mowlem, M.C., Anesio, A.M., Stibal, M., 2019. Greenland melt drives continuous export of methane from the ice-sheet bed. Nature 565 (7737), 73-+.
Li, F.P., Zhang, Y.Q., Xu, Z.X., Teng, J., Liu, C.M., Liu, W.F., Mpelasoka, F., 2013. The impact of climate change on runoff in the southeastern Tibetan Plateau. J. Hydrol. 505, 188–201.
Li, S.Y., Bush, R.T., Santos, I.R., Zhang, Q.F., Song, K.S., Mao, R., Wen, Z.D., Lu, X.X., 2018a. Large greenhouse gases emissions from China's lakes and reservoirs. Water Res. 147, 13–24.
Li, X.Y., Ding, Y.J., Xu, J.Z., He, X.B., Han, T.D., Kang, S.C., Wu, Q.B., Mika, S., Yu, Z.B., Li, Q.J., 2018b. Importance of mountain glaciers as a source of dissolved organic carbon. J. Geophys. Res. Earth Surf. 123 (9), 2123–2134.
Li, M.X., Peng, C.H., Zhou, X.L., Yang, Y.Z., Guo, Y.R., Shi, G.H., Zhu, Q.A., 2019a. Modeling global riverine DOC flux dynamics from 1951 to 2015. J. Adv. Model. Earth Syst. 11 (2), 514–530.
Li, Q.L., Wang, N.L., Barbante, C., Kang, S.C., Callegaro, A., Battistel, D., Argiriadis, E., Wan, X., Yao, P., Pu, T., Wu, X.B., Han, Y., Huai, Y.P., 2019b. Biomass burning source identification through molecular markers in cryoconites over the Tibetan Plateau. Environ. Pollut. 244, 209–217.
Li, H.J., Li, H.Y., Wang, J., Hao, X.H., 2020a. Monitoring high-altitude river ice distribution at the basin scale in the northeastern Tibetan Plateau from a Landsat time-series spanning 1999-2018. Remote Sens. Environ. 247.
Li, Z.X., Li, Z.J., Feng, Q., Zhang, B.J., Gui, J., Xue, J., Gao, W.D., 2020b. Runoff dominated by supra-permafrost water in the source region of the Yangtze river using environmental isotopes. J. Hydrol. 582.
Li, M.X., Peng, C.H., Zhang, K.R., Xu, L., Wang, J.M., Yang, Y., Li, P., Liu, Z.L., He, N.P., 2021a. Headwater stream ecosystem: an important source of greenhouse gases to the atmosphere. Water Res. 190.
Li, Y., Kang, S.C., Zhang, X.L., Chen, J.Z., Schmale, J., Li, X.F., Zhang, Y.L., Niu, H.W., Li, Z.Q., Qin, X., He, X.B., Yang, W., Zhang, G.S., Wang, S.J., Shao, L.L., Tian, L.D., 2021b. Black carbon and dust in the Third Pole glaciers: Revaluated concentrations, mass absorption cross-sections and contributions to glacier ablation. Sci. Total Environ. 789.
Li, Z., Wang, Y.B., Herzschuh, U., Cao, X.Y., Ni, J., Zhao, Y., 2021c. Pollen-based mapping of Holocene vegetation on the Qinghai-Tibetan Plateau in response to climate change. Palaeogeogr. Palaeoclimatol. Palaeoecol. 573.
Li, X.Y., Long, D., Scanlon, B.R., Mann, M.E., Li, X.D., Tian, F.Q., Sun, Z.L., Wang, G.Q., 2022a. Climate change threatens terrestrial water storage over the Tibetan Plateau. Nature. Climate Change 12 (9), 801-+.
Li, X.Y., Shi, F.Z., Ma, Y.J., Zhao, S.J., Wei, J.Q., 2022b. Significant winter CO2 uptake by saline lakes on the Qinghai-Tibet Plateau. Glob. Chang. Biol. 28 (6), 2041–2052.
Li, X.Y., Wang, N.L., Ding, Y.J., Hawkings, J.R., Yde, J.C., Raiswell, R., Liu, J.T., Zhang, S.Q., Kang, S.C., Wang, R.J., Liu, Q., Liu, S.Y., Bol, R., You, X.N., Li, G.Y., 2022c. Globally elevated chemical weathering rates beneath glaciers. Nat. Commun. 13 (1).
Lin, P.L., Du, Z.H., Wang, L., Liu, J.F., Xu, Q., Du, J., Jiang, R., 2023. Hotspots of riverine greenhouse gas (CH4, CO2, N2O) emissions from Qinghai Lake Basin on the northeast Tibetan Plateau. Sci. Total Environ. 857.
Liu, Y., Chen, H.P., 2022. Future warming accelerates lake variations inthe Tibetan Plateau. Int. J. Climatol. 42 (16), 8687–8700.
Liu, Y.M., Xu, J.Z., Kang, S.C., Li, X.F., Li, Y., 2016. Storage of dissolved organic carbon in Chinese glaciers. J. Glaciol. 62 (232), 402–406.
Liu, Y.Q., Vick-Majors, T.J., Priscu, J.C., Yao, T.D., Kang, S.C., Liu, K.S., Cong, Z.Y., Xiong, J.B., Li, Y., 2017. Biogeography of cryoconite bacterial communities on glaciers of the Tibetan Plateau. FEMS Microbiol. Ecol. 93 (6).
Liu, F.T., Chen, L.Y., Abbott, B.W., Xu, Y.P., Yang, G.B., Kou, D., Qin, S.Q., Strauss, J., Wang, Y.H., Zhang, B.B., Yang, Y.H., 2018. Reduced quantity and quality of SOM along a thaw sequence on the Tibetan Plateau. Environ. Res. Lett. 13 (10).
Liu, Y.W., Wei, D., Tenzintarchen, Zhao, J.X., Geng, X.D., Dai, D.X., Xu, R., 2021. Nitrogen addition alters C-N cycling in alpine rangelands: evidence from a 4-year in situ field experiment. Catena 203.
Liu, F.T., Qin, S.Q., Fang, K., Chen, L.Y., Peng, Y.F., Smith, P., Yang, Y.H., 2022a. Divergent changes in particulate and mineral-associated organic carbon upon permafrost thaw. Nat. Commun. 13 (1).
Liu, Y.Q., Ji, M.K., Yu, T., Zaugg, J.L., Anesio, A.M., Zhang, Z.H., Hu, S.N., Hugenholtz, P., Liu, K.S., Liu, P.F., Chen, Y.Y., Luo, Y.F., Yao, T.D., 2022b. A genome and gene catalog of glacier microbiomes. Nat. Biotechnol. 40 (9), 1341-+.
Lu, Q., Zhao, D.S., Wu, S.H., 2017. Simulated responses of permafrost distribution to climate change on the Qinghai-Tibet Plateau. Sci. Rep. 7.
Luo, J., Niu, F.J., Lin, Z.J., Liu, M.H., Yin, G.A., Gao, Z.Y., 2022. Abrupt increase in thermokarst lakes on the central Tibetan Plateau over the last 50 years. Catena 217.
MacDougall, A.H., Avis, C.A., Weaver, A.J., 2012. Significant contribution to climate warming from the permafrost carbon feedback. Nat. Geosci. 5 (10), 719–721.
Manning, C.C., Preston, V.L., Jones, S.F., Michel, A.P.M., Nicholson, D.P., Duke, P.J., Ahmed, M.M.M., Manganini, K., Else, B.G.T., Tortell, P.D., 2020. River Inflow Dominates methane Emissions in an Arctic Coastal System. Geophys. Res. Lett. 47 (10).
McGuire, A.D., Koven, C., Lawrence, D.M., Clein, J.S., Xia, J.Y., Beer, C., Burke, E., Chen, G.S., Chen, X.D., Delire, C., Jafarov, E., MacDougall, A.H., Marchenko, S., Nicolsky, D., Peng, S.S., Rinke, A., Saito, K., Zhang, W.X., Alkama, R., Bohn, T.J., Ciais, P., Decharme, B., Ekici, A., Gouttevin, I., Hajima, T., Hayes, D.J., Ji, D.Y., Krinner, G., Lettenmaier, D.P., Luo, Y.Q., Miller, P.A., Moore, J.C., Romanovsky, V., Schadel, C., Schaefer, K., Schuur, E.A.G., Smith, B., Sueyoshi, T., Zhuang, Q.L., 2016. Variability in the sensitivity among model simulations of permafrost and carbon dynamics in the permafrost region between 1960 and 2009. Glob. Biogeochem. Cycles 30 (7), 1015–1037.
Miehe, G., Schleuss, P.M., Seeber, E., Babel, W., Biermann, T., Braendle, M., Chen, F.H., Coners, H., Foken, T., Gerken, T., Graf, H.F., Guggenberger, G., Hafner, S., Holzapfel, M., Ingrisch, J., Kuzyakov, Y., Lai, Z.P., Lehnert, L., Leuschner, C., Li, X. G., Liu, J.Q., Liu, S.B., Ma, Y.M., Miehe, S., Mosbrugger, V., Noltie, H.J., Schmidt, J., Spielvogel, S., Unteregelsbacher, S., Wang, Y., Willinghofer, S., Xu, X.L., Yang, Y.P., Zhang, S.R., Opgenoorth, L., Wesche, K., 2019. The Kobresia pygmaea ecosystem of the Tibetan highlands - Origin, functioning and degradation of the world's largest pastoral alpine ecosystem Kobresia pastures of Tibet. Sci. Total Environ. 648, 754–771.
Miles, E., McCarthy, M., Dehecq, A., Kneib, M., Fugger, S., Pellicciotti, F., 2021. Health and sustainability of glaciers in High Mountain Asia. Nat. Commun. 12 (1).
Miner, K.R., D'Andrilli, J., Mackelprang, R., Edwards, A., Malaska, M.J., Waldrop, M.P., Miller, C.E., 2021. Emergent biogeochemical risks from Arctic permafrost degradation. Nat. Clim. Chang. 11 (10), 809–819.
Miner, K.R., Turetsky, M.R., Malina, E., Bartsch, A., Tamminen, J., McGuire, A.D., Fix, A., Sweeney, C., Elder, C.D., Miller, C.E., 2022. Permafrost carbon emissions in a changing Arctic. Nat. Rev. Earth Environ. 3 (1), 55–67.
Mishra, U., Hugelius, G., Shelef, E., Yang, Y., Strauss, J., Lupachev, A., Harden, J.W., Jastrow, J.D., Ping, C.-L., Riley, W.J., 2021a. Spatial heterogeneity and environmental predictors of permafrost region soil organic carbon stocks. Sci. Adv. 7 (9), eaaz5236.
Mishra, U., Hugelius, G., Shelef, E., Yang, Y.H., Strauss, J., Lupachev, A., Harden, J.W., Jastrow, J.D., Ping, C.L., Riley, W.J., Schuur, E.A.G., Matamala, R., Siewert, M., Nave, L.E., Koven, C.D., Fuchs, M., Palmtag, J., Kuhry, P., Treat, C.C., Zubrzycki, S., Hoffman, F.M., Elberling, B., Camill, P., Veremeeva, A., Orr, A., 2021b. Spatial heterogeneity and environmental predictors of permafrost region soil organic carbon stocks. Sci. Adv. 7 (9).
Mu, C.C., Zhang, T.J., Zhang, X.K., Li, L.L., Guo, H., Zhao, Q., Cao, L., Wu, Q.B., Cheng, G.D., 2016. Carbon loss and chemical changes from permafrost collapse in the northern Tibetan Plateau. J. Geophys. Res Biogeosci. 121 (7), 1781–1791.
Mu, C.C., Li, L.L., Wu, X.D., Zhang, F., Jia, L., Zhao, Q., Zhang, T.J., 2018. Greenhouse gas released from the deep permafrost in the northern Qinghai-Tibetan Plateau. Sci. Rep. 8.
Mu, C.C., Abbott, B.W., Norris, A.J., Mu, M., Fan, C.Y., Chen, X., Jia, L., Yang, R.M., Zhang, T.J., Wang, K., Peng, X.Q., Wu, Q.B., Guggenberger, G., Wu, X.D., 2020. The status and stability of permafrost carbon on the Tibetan Plateau. Earth Sci. Rev. 211.
Mu, C.C., Mu, M., Wu, X.D., Jia, L., Fan, C.Y., Peng, X.Q., Ping, C.L., Wu, Q.B., Xiao, C.D., Liu, J.B., 2023. High carbon emissions from thermokarst lakes and their determinants in the Tibet Plateau. Glob. Chang. Biol. 29 (10), 2732–2745.
Natali, S.M., Holdren, J.P., Rogers, B.M., Treharne, R., Duffy, P.B., Pomerance, R., MacDonald, E., 2021. Permafrost carbon feedbacks threaten global climate goals. Proc. Natl. Acad. Sci. USA 118 (21).
Nie, Y., Pritchard, H.D., Liu, Q., Hennig, T., Wang, W.L., Wang, X.M., Liu, S.Y., Nepal, S., Samyn, D., Hewitt, K., Chen, X.Q., 2021. Glacial change and hydrological implications in the Himalaya and Karakoram. Nat. Rev. Earth Environ. 2 (2), 91–106.
Nitze, I., Grosse, G., Jones, B.M., Romanovsky, V.E., Boike, J., 2018. Remote sensing quantifies widespread abundance of permafrost region disturbances across the Arctic and Subarctic. Nat. Commun. 9.
Niu, H.W., Kang, S.C., Lu, X.X., Shi, X.F., 2018. Distributions and light absorption property of water soluble organic carbon in a typical temperate glacier, southeastern Tibetan Plateau. Tellus Ser. B 70.
Olefeldt, D., Goswami, S., Grosse, G., Hayes, D., Hugelius, G., Kuhry, P., McGuire, A.D., Romanovsky, V.E., Sannel, A.B.K., Schuur, E.A.G., Turetsky, M.R., 2016. Circumpolar distribution and carbon storage of thermokarst landscapes. Nat. Commun. 7.
Olid, C., Rodellas, V., Rocher-Ros, G., Garcia-Orellana, J., Diego-Feliu, M., Alorda-Kleinglass, A., Bastviken, D., Karlsson, J., 2022. Groundwater discharge as a driver of methane emissions from Arctic lakes. Nat. Commun. 13 (1).
Qin, S.Q., Kou, D., Mao, C., Chen, Y.L., Chen, L.Y., Yang, Y.H., 2021. Temperature sensitivity of permafrost carbon release mediated by mineral and microbial properties. Sci. Adv. 7 (32).
Qu, B., Aho, K.S., Li, C.L., Kang, S.C., Sillanpaa, M., Yan, F.P., Raymond, P.A., 2017a. Greenhouse gases emissions in rivers of the Tibetan Plateau. Sci. Rep. 7.
Qu, B., Sillanpaa, M., Li, C.L., Kang, S.C., Stubbins, A., Yan, F.P., Aho, K.S., Zhou, F., Raymond, P.A., 2017b. Aged dissolved organic carbon exported from rivers of the Tibetan Plateau. PLoS One 12 (5).
Ran, L.S., Lu, X.X., Yang, H., Li, L.Y., Yu, R.H., Sun, H.G., Han, J.T., 2015. CO2 outgassing from the Yellow River network and its implications for riverine carbon cycle. J. Geophys. Res Biogeosci. 120 (7), 1334–1347.
Raymond, P.A., Bauer, J.E., 2001. Riverine export of aged terrestrial organic matter to the North Atlantic Ocean. Nature 409 (6819), 497–500.
Raymond, P.A., Hartmann, J., Lauerwald, R., Sobek, S., McDonald, C., Hoover, M., Butman, D., Striegl, R., Mayorga, E., Humborg, C., Kortelainen, P., Durr, H., Meybeck, M., Ciais, P., Guth, P., 2013. Global carbon dioxide emissions from inland waters. Nature 503 (7476), 355–359.
RGI, 2017. Randolph Glacier Inventory – A Dataset of Global Glacier Outlines: Version 6.0. Technical Report, Colorado, USA.
Rosentreter, J.A., Borges, A.V., Deemer, B.R., Holgerson, M.A., Liu, S.D., Song, C.L., Melack, J., Raymond, P.A., Duarte, C.M., Allen, G.H., Olefeldt, D., Poulter, B., Battin, T.I., Eyre, B.D., 2021. Half of global methane emissions come from highly variable aquatic ecosystem sources. Nat. Geosci. 14 (4), 225–+.

Sanches, L.F., Guenet, B., Marinho, C.C., Barros, N., Esteves, F.D., 2019. Global regulation of methane emission from natural lakes. Sci. Rep. 9.
Saunois, M., Stavert, A.R., Poulter, B., Bousquet, P., Canadell, J.G., Jackson, R.B., Raymond, P.A., Dlugokencky, E.J., Houweling, S., Patra, P.K., Ciais, P., Arora, V.K., Bastviken, D., Bergamaschi, P., Blake, D.R., Brailsford, G., Bruhwiler, L., Carlson, K. M., Carrol, M., Castaldi, S., Chandra, N., Crevoisier, C., Crill, P.M., Covey, K., Curry, C.L., Etiope, G., Frankenberg, C., Gedney, N., Hegglin, M.I., Hoglund-Isaksson, L., Hugelius, G., Ishizawa, M., Ito, A., Janssens-Maenhout, G., Jensen, K.M., Joos, F., Kleinen, T., Krummel, P.B., Langenfelds, R.L., Laruelle, G.G., Liu, L.C., Machida, T., Maksyutov, S., McDonald, K.C., McNorton, J., Miller, P.A., Melton, J.R., Morino, I., Muller, J., Murguia-Flores, F., Naik, V., Niwa, Y., Noce, S., Doherty, S.O., Parker, R.J., Peng, C.H., Peng, S.S., Peters, G.P., Prigent, C., Prinn, R., Ramonet, M., Regnier, P., Riley, W.J., Rosentreter, J.A., Segers, A., Simpson, I.J., Shi, H., Smith, S. J., Steele, L.P., Thornton, B.F., Tian, H.Q., Tohjima, Y., Tubiello, F.N., Tsuruta, A., Viovy, N., Voulgarakis, A., Weber, T.S., van Weele, M., van der Werf, G.R., Weiss, R. F., Worthy, D., Wunch, D., Yin, Y., Yoshida, Y., Zhang, W.X., Zhang, Z., Zhao, Y.H., Zheng, B., Zhu, Q., Zhu, Q.A., Zhuang, Q.L., 2020. The global methane budget 2000-2017. Earth Syst. Sci. Data 12 (3), 1561–1623.
Sawstrom, C., Mumford, P., Marshall, W., Hodson, A., Laybourn-Parry, J., 2002. The microbial communities and primary productivity of cryoconite holes in an Arctic glacier (Svalbard 79 degrees N). Polar Biol. 25 (8), 591–596.
Schuur, E.A.G., Vogel, J.G., Crummer, K.G., Lee, H., Sickman, J.O., Osterkamp, T.E., 2009. The effect of permafrost thaw on old carbon release and net carbon exchange from tundra. Nature 459 (7246), 556–559.
Schuur, E.A.G., Abbott, B.W., Bowden, W.B., Brovkin, V., Camill, P., Canadell, J.G., Chanton, J.P., Chapin, F.S., Christensen, T.R., Ciais, P., Crosby, B.T., Czimczik, C.I., Grosse, G., Harden, J., Hayes, D.J., Hugelius, G., Jastrow, J.D., Jones, J.B., Kleinen, T., Koven, C.D., Krinner, G., Kuhry, P., Lawrence, D.M., McGuire, A.D., Natali, S.M., O'Donnell, J.A., Ping, C.L., Riley, W.J., Rinke, A., Romanovsky, V.E., Sannel, A.B.K., Schadel, C., Schaefer, K., Sky, J., Subin, Z.M., Tarnocai, C., Turetsky, M.R., Waldrop, M.P., Anthony, K.M.W., Wickland, K.P., Wilson, C.J., Zimov, S.A., 2013. Expert assessment of vulnerability of permafrost carbon to climate change. Clim. Chang. 119 (2), 359–374.
Schuur, E.A.G., McGuire, A.D., Schadel, C., Grosse, G., Harden, J.W., Hayes, D.J., Hugelius, G., Koven, C.D., Kuhry, P., Lawrence, D.M., Natali, S.M., Olefeldt, D., Romanovsky, V.E., Schaefer, K., Turetsky, M.R., Treat, C.C., Vonk, J.E., 2015. Climate change and the permafrost carbon feedback. Nature 520 (7546), 171–179.
Schuur, E.A.G., Abbott, B.W., Commane, R., Ernakovich, J., Euskirchen, E., Hugelius, G., Grosse, G., Jones, M., Koven, C., Leshyk, V., Lawrence, D., Loranty, M.M., Mauritz, M., Olefeldt, D., Natali, S., Rodenhizer, H., Salmon, V., Schadel, C., Strauss, J., Treat, C., Turetsky, M., 2022. Permafrost and climate change: carbon cycle feedbacks from the warming arctic. Annu. Rev. Environ. Resour. 47, 343–371.
Semiletov, I.P., 1999. Aquatic sources and sinks of CO2 and CH4 in the polar regions. J. Atmos. Sci. 56 (2), 286–306.
Serikova, S., Pokrovsky, O.S., Laudon, H., Krickov, I.V., Lim, A.G., Manasypov, R.M., Karlsson, J., 2019. High carbon emissions from thermokarst lakes of Western Siberia. Nat. Commun. 10.
Shean, D.E., Bhushan, S., Montesano, P., Rounce, D.R., Arendt, A., Osmanoglu, B., 2020. A Systematic, Regional Assessment of High Mountain Asia Glacier Mass Balance. Front. Earth Sci. 7.
Shen, M.G., Piao, S.L., Jeong, S.J., Zhou, L.M., Zeng, Z.Z., Ciais, P., Chen, D.L., Huang, M. T., Jin, C.S., Li, L.Z.X., Li, Y., Myneni, R.B., Yang, K., Zhang, G.X., Zhang, Y.J., Yao, T.D., 2015. Evaporative cooling over the Tibetan Plateau induced by vegetation growth. Proc. Natl. Acad. Sci. USA 112 (30), 9299–9304.
Shen, T.Q., Jiang, P., Ju, Q., Yu, Z.B., Chen, X.G., Lin, H., Zhang, Y.G., 2023. Changes in permafrost spatial distribution and active layer thickness from 1980 to 2020 on the Tibet Plateau. Sci. Total Environ. 859.
Shiklomanov, A.I., Lammers, R.B., 2014. River ice responses to a warming Arctic-recent evidence from Russian rivers. Environ. Res. Lett. 9 (3).
Song, C.L., Wang, G.X., Sun, X.Y., Li, Y., Ye, S.L., Hu, Z.Y., Sun, J.Y., Lin, S., 2023. Riverine CO2 variations in permafrost catchments of the Yangtze River source region: Hot spots and hot moments. Sci. Total Environ. 863.
Stanley, E.H., Powers, S.M., Lottig, N.R., Buffam, I., Crawford, J.T., 2012. Contemporary changes in dissolved organic carbon (DOC) in human-dominated rivers: is there a role for DOC management? Freshw. Biol. 57, 26–42.
Sun, R., Zhang, X.Q., Fraedrich, K., You, Q.L., 2021. CMIP5 climate projections for the Yamzhog Yumco Basin: an environmental testbed for alpine lakes. Theor. Appl. Climatol. 143 (1–2), 795–808.
Turetsky, M.R., Abbott, B.W., Jones, M.C., Anthony, K.W., Olefeldt, D., Schuur, E.A.G., Koven, C., McGuire, A.D., Grosse, G., Kuhry, P., Hugelius, G., Lawrence, D.M., Gibson, C., Sannel, A.B.K., 2019. Permafrost collapse is accelerating carbon release. Nature 569 (7754), 32–34.
Turetsky, M.R., Abbott, B.W., Jones, M.C., Anthony, K.W., Olefeldt, D., Schuur, E.A.G., Grosse, G., Kuhry, P., Hugelius, G., Koven, C., Lawrence, D.M., Gibson, C., Sannel, A. B.K., McGuire, A.D., 2020. Carbon release through abrupt permafrost thaw. Nat. Geosci. 13 (2), 138-+.
Vonk, J.E., Gustafsson, O., 2013. Permafrost-carbon complexities. Nat. Geosci. 6 (9), 675–676.
Vonk, J.E., Tank, S.E., Bowden, W.B., Laurion, I., Vincent, W.F., Alekseychik, P., Amyot, M., Billet, M.F., Canario, J., Cory, R.M., Deshpande, B.N., Helbig, M., Jammet, M., Karlsson, J., Larouche, J., MacMillan, G., Rautio, M., Anthony, K.M.W., Wickland, K.P., 2015. Reviews and syntheses: Effects of permafrost thaw on Arctic aquatic ecosystems. Biogeosciences 12 (23), 7129–7167.
Wadham, J.L., Arndt, S., Tulaczyk, S., Stibal, M., Tranter, M., Telling, J., Lis, G.P., Lawson, E., Ridgwell, A., Dubnick, A., Sharp, M.J., Anesio, A.M., Butler, C.E.H., 2012. Potential methane reservoirs beneath Antarctica. Nature 488 (7413), 633–637.
Wang, T.H., Yang, D.W., Yang, Y.T., Piao, S.L., Li, X., Cheng, G.D., Fu, B.J., 2020. Permafrost thawing puts the frozen carbon at risk over the Tibetan Plateau. Sci. Adv. 6 (19).
Wang, D., Wu, T.H., Zhao, L., Mu, C.C., Li, R., Wei, X.H., Hu, G.J., Zou, D.F., Zhu, X.F., Chen, J., Hao, J.M., Ni, J., Li, X.F., Ma, W.S., Wen, A.M., Shang, C.P., La, Y.N., Ma, X., Wu, X.D., 2021a. A 1 km resolution soil organic carbon dataset for frozen ground in the Third Pole. Earth Syst. Sci. Data 13 (7), 3453–3465.
Wang, L., Du, Z.H., Wei, Z.Q., Xu, Q., Feng, Y.R., Lin, P.L., Lin, J.H., Chen, S.Y., Qiao, Y. P., Shi, J.Z., Xiao, C.D., 2021b. High methane emissions from thermokarst lakes on the Tibetan Plateau are largely attributed to ebullition fluxes. Sci. Total Environ. 801.
Wang, L., Yao, T.D., Chai, C.H., Cuo, L., Su, F.G., Zhang, F., Yao, Z.J., Zhang, Y.S., Li, X. P., Qi, J., Hu, Z.D., Liu, J.S., Wang, Y.W., 2021c. TP-River: monitoring and quantifying total river runoff from the Third Pole. Bull. Am. Meteorol. Soc. 102 (5), E948–E965.
Wang, M., Xu, B.Q., Wang, H.L., Zhang, R.D., Yang, Y., Gao, S.P., Tang, X.X., Wang, N.L., 2021d. Black carbon deposited in Hariqin Glacier of the Central Tibetan Plateau record changes in the emission from Eurasia. Environ. Pollut. 273.
Wang, L., Xiao, C.D., Du, Z.H., Maher, D.T., Liu, J.F., Wei, Z.Q., 2022a. In-situ measurement on air-water flux of CH4, CO2 and their carbon stable isotope in lakes of northeast Tibetan Plateau. Adv. Clim. Chang. Res. 13 (2), 279–289.
Wang, X.J., Ran, Y.H., Pang, G.J., Chen, D.L., Su, B., Chen, R., Li, X., Chen, H.W., Yang, M.X., Gou, X.H., Jorgenson, M.T., Aalto, J., Li, R., Peng, X.Q., Wu, T.H., Clow, G.D., Wan, G.N., Wu, X.D., Luo, D.L., 2022b. Contrasting characteristics, changes, and linkages of permafrost between the Arctic and the Third Pole. Earth Sci. Rev. 230.
Wang, T.H., Yang, D.W., Yang, Y.T., Zheng, G.H., Jin, H.J., Li, X., Yao, T.D., Cheng, G.D., 2023. Unsustainable water supply from thawing permafrost on the Tibetan Plateau in a changing climate. Sci. Bull. 68 (11), 1105–1108.
Wei, D., Xu, R., Wang, Y.H., Wang, Y.S., Liu, Y.W., Yao, T.D., 2012. Responses of CO2, CH4 and N2O fluxes to livestock exclosure in an alpine steppe on the Tibetan Plateau, China. Plant Soil 359 (1–2), 45–55.
Wei, D., Xu, R., Tenzin, T., Wang, Y.S., Wang, Y.H., 2015. Considerable methane uptake by alpine grasslands despite the cold climate: in situ measurements on the central Tibetan Plateau, 2008-2013. Glob. Chang. Biol. 21 (2), 777–788.
Wei, D., Zhao, H., Zhang, J.X., Qi, Y.H., Wang, X.D., 2020. Human activities alter response of alpine grasslands on Tibetan Plateau to climate change. J. Environ. Manag. 262.
Wei, D., Qi, Y., Ma, Y., Wang, X., 2021a. Plant uptake of CO2 outpaces losses from permafrost and plant respiration on the Tibetan Plateau. Proc. Natl. Acad. Sci. USA.
Wei, D., Qi, Y.H., Ma, Y.M., Wang, X.F., Ma, W.Q., Gao, T.G., Huang, L., Zhao, H., Zhang, J.X., Wang, X.D., 2021b. Plant uptake of CO2 outpaces losses from permafrost and plant respiration on the Tibetan Plateau. Proc. Natl. Acad. Sci. USA 118 (33).
Wei, Z.Q., Du, Z.H., Wang, L., Lin, J.H., Feng, Y.R., Xu, Q., Xiao, C.D., 2021c. Sentinel-based inventory of Thermokarst Lakes and Ponds across permafrost landscapes on the Qinghai-Tibet Plateau. Earth Space Sci. 8 (11).
Wei, Z.Q., Du, Z.H., Wang, L., Zhong, W., Lin, J.H., Xu, Q., Xiao, C.D., 2022. Sedimentary organic carbon storage of thermokarst lakes and ponds across Tibetan permafrost region. Sci. Total Environ. 831.
Weiss, N., Blok, D., Elberling, B., Hugelius, G., Jorgensen, C.J., Siewert, M.B., Kuhry, P., 2016. Thermokarst dynamics and soil organic matter characteristics controlling initial carbon release from permafrost soils in the Siberian Yedoma region. Sediment. Geol. 340, 38–48.
Wen, Z.D., Song, K.S., Shang, Y.X., Fang, C., Li, L., Lv, L.L., Lv, X.G., Chen, L.J., 2017. Carbon dioxide emissions from lakes and reservoirs of China: a regional estimate based on the calculated pCO(2). Atmos. Environ. 170, 71–81.
Wu, T.H., Wang, D., Mu, C.C., Zhang, W.X., Zhu, X.F., Zhao, L., Li, R., Hu, G.J., Zou, D.F., Chen, J., Wei, X.H., Wen, A.M., Shang, C.P., La, Y.N., Lou, P.Q., Ma, X., Wu, X.D., 2022. Storage, patterns, and environmental controls of soil organic carbon stocks in the permafrost regions of the Northern Hemisphere. Sci. Total Environ. 828.
Xu, H., Li, Z., Nozomu, T., Zhang, X., Luo, S., 2014. Characteristics and formation analysis of cryoconite granules of Yushugou Glacier. Arid Land Geogr. 37 (3), 429–438.
Xun, F., Li, B., Chen, H., Zhou, Y.Q., Gao, P.X., Xing, P., 2022. Effect of salinity in Alpine Lakes on the Southern Tibetan Plateau on greenhouse gas diffusive fluxes. J. Geophys. Res Biogeosci. 127 (7).
Yan, F.P., Kang, S.C., Li, C.L., Zhang, Y.L., Qin, X., Li, Y., Zhang, X.P., Hu, Z.F., Chen, P.F., Li, X.F., Qu, B., Sillanpaa, M., 2016. Concentration, sources and light absorption characteristics of dissolved organic carbon on a medium-sized valley glacier, northern Tibetan Plateau. Cryosphere 10 (6), 2611–2621.
Yan, F.P., Sillanpaa, M., Kang, S.C., Aho, K.S., Qu, B., Wei, D., Li, X.F., Li, C.L., Raymond, P.A., 2018. Lakes on the Tibetan Plateau as conduits of greenhouse gases to the atmosphere. J. Geophys. Res Biogeosci. 123 (7), 2091–2103.
Yan, F.P., Du, Z.H., Pu, T., Xu, Q., Wang, L., Ma, R.F., Zhang, C., Li, C.L., Kang, S.C., 2023. Isotopic composition and emission characteristics of CO2 and CH4 in glacial lakes of the Tibetan Plateau. Environ. Res. Lett. 18 (9), 094025.
Yang, G.B., Peng, Y.F., Olefeld, D., Chen, Y.L., Wang, G.Q., Li, F., Zhang, D.Y., Wang, J., Yu, J.C., Liu, L., Qin, S.Q., Sun, T.Y., Yang, Y.H., 2018. Changes in methane flux along a permafrost thaw sequence on the Tibetan Plateau. Environ. Sci. Technol. 52 (3), 1244–1252.
Yang, M.X., Wang, X.J., Pang, G.J., Wang, G.N., Liu, Z.C., 2019. The Tibetan Plateau cryosphere: observations and model simulations for current status and recent changes. Earth Sci. Rev. 190, 353–369.

Yang, G., Zheng, Z., Abbott, B.W., Olefeldt, D., Knoblauch, C., Song, Y., Kang, L., Qin, S., Peng, Y., Yang, Y., 2023. Characteristics of methane emissions from alpine thermokarst lakes on the Tibetan Plateau. Nat. Commun. 14 (1), 3121.
Yao, T.D., Thompson, L., Yang, W., Yu, W.S., Gao, Y., Guo, X.J., Yang, X.X., Duan, K.Q., Zhao, H.B., Xu, B.Q., Pu, J.C., Lu, A.X., Xiang, Y., Kattel, D.B., Joswiak, D., 2012. Different glacier status with atmospheric circulations in Tibetan Plateau and surroundings. Nat. Clim. Chang. 2 (9), 663–667.
Yao, T.D., Xue, Y.K., Chen, D.L., Chen, F.H., Thompson, L., Cui, P., Koike, T., Lau, W.K. M., Lettenmaier, D., Mosbrugger, V., Zhang, R.H., Xu, B.Q., Dozier, J., Gillespie, T., Gu, Y., Kang, S.C., Piao, S.L., Sugimoto, S., Ueno, K., Wang, L., Wang, W.C., Zhang, F., Sheng, Y.W., Guo, W.D., Ailikun, Yang, X.X., Ma, Y.M., Shen, S.S.P., Su, Z. B., Chen, F., Liang, S.L., Liu, Y.M., Singh, V.P., Yang, K., Yang, D.Q., Zhao, X.Q., Qian, Y., Zhang, Y., Li, Q., 2019. Recent Third Pole's rapid warming accompanies cryospheric melt and water cycle intensification and interactions between monsoon and environment: multidisciplinary approach with observations, modeling, and analysis. Bull. Am. Meteorol. Soc. 100 (3), 423–444.
Yao, T.D., Bolch, T., Chen, D.L., Gao, J., Immerzeel, W., Piao, S., Su, F.G., Thompson, L., Wada, Y., Wang, L., Wang, T., Wu, G.J., Xu, B.Q., Yang, W., Zhang, G.Q., Zhao, P., 2022. The imbalance of the Asian water tower. Nat. Rev. Earth Environ. 3 (10), 618–632.
You, X.N., Li, X.Y., 2021. Seasonal variations in dissolved organic carbon in the Source Region of the Yellow River on the Tibetan Plateau. Water 13 (20).
You, Q.L., Cai, Z.Y., Pepin, N., Chen, D.L., Ahrens, B., Jiang, Z.H., Wu, F.Y., Kang, S.C., Zhang, R.N., Wu, T.H., Wang, P.L., Li, M.C., Zuo, Z.Y., Gao, Y.H., Zhai, P.M., Zhang, Y.Q., 2021. Warming amplification over the Arctic Pole and Third Pole: trends, mechanisms and consequences. Earth Sci. Rev. 217.
You, X.N., Li, X.Y., Sillanpaa, M., Wang, R., Wu, C.Y., Xu, Q.Q., 2022. Export of dissolved organic carbon from the source region of Yangtze River in the Tibetan Plateau. Sustainability 14 (4).
Zhang, Y.L., Kang, S.C., Cong, Z.Y., Schmale, J., Sprenger, M., Li, C.L., Yang, W., Gao, T. G., Sillanpaa, M., Li, X.F., Liu, Y.J., Chen, P.F., Zhang, X.L., 2017a. Light-absorbing impurities enhance glacier albedo reduction in the southeastern Tibetan plateau. J. Geophys. Res.-Atmos. 122 (13), 6915–6933.
Zhang, Y.L., Kang, S.C., Li, C.L., Gao, T.G., Cong, Z.Y., Sprenger, M., Liu, Y.J., Li, X.F., Guo, J.M., Sillanpaa, M., Wang, K., Chen, J.Z., Li, Y., Sun, S.W., 2017b. Characteristics of black carbon in snow from Laohugou No. 12 glacier on the northern Tibetan Plateau. Sci. Total Environ. 607, 1237–1249.
Zhang, G.Q., Luo, W., Chen, W.F., Zheng, G.X., 2019. A robust but variable lake expansion on the Tibetan Plateau. Sci. Bull. 64 (18), 1306–1309.
Zhang, L.W., Xia, X.H., Liu, S.D., Zhang, S.B., Li, S.L., Wang, J.F., Wang, G.Q., Gao, H., Zhang, Z.R., Wang, Q.R., Wen, W., Liu, R., Yang, Z.F., Stanley, E.H., Raymond, P.A., 2020. Significant methane ebullition from alpine permafrost rivers on the East Qinghai-Tibet Plateau. Nat. Geosci. 13 (5), 349–354.
Zhang, Y.L., Gao, T.G., Kang, S.C., Shangguan, D.H., Luo, X., 2021a. Albedo reduction as an important driver for glacier melting in Tibetan Plateau and its surrounding areas. Earth Sci. Rev. 220.
Zhang, Y.L., Kang, S.C., Wei, D., Luo, X., Wang, Z.Z., Gao, T.G., 2021b. Sink or source? Methane and carbon dioxide emissions from cryoconite holes, subglacial sediments, and proglacial river runoffduring intensive glacier melting on the Tibetan Plateau. Fundam. Res. 1, 232–239.
Zhang, T.G., Wang, W.C., An, B.S., Gao, T.G., Yao, T.D., 2022. Ice thickness and morphological analysis reveal the future glacial lake distribution and formation probability in the Tibetan Plateau and its surroundings. Glob. Planet. Chang. 216.
Zhao, L., Wu, X.D., Wang, Z.W., Sheng, Y., Fang, H.B., Zhao, Y.H., Hu, G.J., Li, W.P., Pang, Q.Q., Shi, J.Z., Mo, B.T., Wang, Q., Ruan, X.R., Li, X.D., Ding, Y.J., 2018. Soil organic carbon and total nitrogen pools in permafrost zones of the Qinghai-Tibetan Plateau. Sci. Rep. 8.
Zhao, L., Zou, D.F., Hu, G.J., Du, E.J., Pang, Q.Q., Xiao, Y., Li, R., Sheng, Y., Wu, X.D., Sun, Z., Wang, L.X., Wang, C., Ma, L., Zhou, H.Y., Liu, S.B., 2020. Changing climate and the permafrost environment on the Qinghai-Tibet (Xizang) plateau. Permafr. Periglac. Process. 31 (3), 396–405.
Zhao, L., Zou, D.F., Hu, G.J., Wu, T.H., Du, E.J., Liu, G.Y., Xiao, Y., Li, R., Pang, Q.Q., Qiao, Y.P., Wu, X.D., Sun, Z., Xing, Z.P., Sheng, Y., Zhao, Y.H., Shi, J.Z., Xie, C.W., Wang, L.X., Wang, C., Cheng, G.D., 2021. A synthesis dataset of permafrost thermal state for the Qinghai-Tibet (Xizang) Plateau, China. Earth Syst. Sci. Data 13 (8), 4207–4218.
Zhao, H.Y., Su, B., Lei, H.J., Zhang, T., Xiao, C.D., 2023. A new projection for glacier mass and runoff changes over High Mountain Asia. Sci. Bull. 68 (1), 43–47.
Zheng, Y.J., Wu, S., Xiao, S.Q., Yu, K., Fang, X.T., Xia, L.L., Wang, J.Y., Liu, S.W., Freeman, C., Zou, J.W., 2022. Global methane and nitrous oxide emissions from inland waters and estuaries. Glob. Chang. Biol. 28 (15), 4713–4725.
Zimov, S.A., Schuur, E.A.G., Chapin, F.S., 2006. Permafrost and the global carbon budget. Science 312 (5780), 1612–1613.
Zou, D.F., Zhao, L., Sheng, Y., Chen, J., Hu, G.J., Wu, T.H., Wu, J.C., Xie, C.W., Wu, X.D., Pang, Q.Q., Wang, W., Du, E.J., Li, W.P., Liu, G.Y., Li, J., Qin, Y.H., Qiao, Y.P., Wang, Z.W., Shi, J.Z., Cheng, G.D., 2017. A new map of permafrost distribution on the Tibetan Plateau. Cryosphere 11 (6), 2527–2542.